From Quarks and Gluons to Hadrons: Chiral Symmetry Breaking in Dynamical QCD

Jens Braun, Leonard Fister, Jan M. Pawlowski, Fabian Rennecke

From Quarks and Gluons to Hadrons: Chiral Symmetry Breaking in Dynamical QCD

Jens Braun,[1,2] Leonard Fister,[3] Jan M. Pawlowski,[4,2] and Fabian Rennecke[4,2]

[1] *Institut für Kernphysik (Theoriezentrum), Technische Universität Darmstadt, Schloßgartenstraße 2, D-64289 Darmstadt, Germany*
[2] *ExtreMe Matter Institute EMMI, GSI, Planckstraße 1, D-64291 Darmstadt, Germany*
[3] *Institut de Physique Théorique, CEA Saclay, F-91191 Gif-sur-Yvette, France*
[4] *Institut für Theoretische Physik, Universität Heidelberg, Philosophenweg 16, 69120 Heidelberg, Germany*

We present an analysis of the dynamics of two-flavour QCD in the vacuum. Special attention is payed to the transition from the high energy quark-gluon regime to the low energy regime governed by hadron dynamics. This is done within a functional renormalisation group approach to QCD amended by dynamical hadronisation techniques. The latter allow us to describe conveniently the transition from the perturbative high-energy regime to the nonperturbative low-energy limit without suffering from a fine-tuning of model parameters. In the present work, we apply these techniques to two-flavour QCD with physical quark masses and show how the dynamics of the dominant low-energy degrees of freedom emerge from the underlying quark-gluon dynamics.

PACS numbers: 12.38.Aw, 11.30.Rd , 12.38.Gc

I. INTRODUCTION

For an accurate first-principles description of the dynamics of QCD, a reliable inclusion of hadronic states is of great importance. This holds in particular for an approach aiming at the hadron spectrum or the phase structure of QCD at finite density. In the present work on two-flavour QCD we develop a theoretical framework for taking into account the fluctuation dynamics of quarks, gluon and hadrons. This approach is based on previous functional renormalisation group studies [1, 2] and a related quantitative study in the quenched limit [3]. The present work and [3] are first works within a collaboration (fQCD) aiming at a quantitative functional renormalisation group framework for QCD [4]. This framework allows to dynamically include hadronic states as they emerge from the microscopic quark and gluon degrees of freedom.

We use the functional renormalisation group (FRG) approach for QCD, for reviews see [5–14], and [15–21] for reviews on related work. In order to describe the transition from quarks and gluons to hadrons, we extend the dynamical hadronisation technique (or rebosonisation), introduced in Refs. [7, 22–24]. For the first time, this technique is applied here to dynamical two-flavour QCD with physical quark masses. It is shown how the dominant hadronic low-energy degrees of freedom and their dynamics emerge from the underlying quark-gluon dynamics. The hadronisation technique, as further developed in the present work, already applied in Ref. [3] in a quantitative study of quenched QCD. In the latter work, a large number of interaction channels has been taken into account, aiming at full quantitative precision. Here, we exploit the results from [3] as well as results on the scale-dependent glue sector of Yang-Mills theory from Refs. [18, 25, 26]. This enables us to concentrate on the RG flows of the most relevant couplings from a more phenomenological point of view, paying special attention to unquenching effects.

In summary, the aim of this work is threefold: Firstly, we aim at a detailed understanding of the fluctuation physics in the transition regime between the high energy quark-gluon phase to the low energy hadronic phase. Secondly, we want to initiate the quest for the minimal set of composite operators that have to be taken into account for reaching (semi-)quantitative precision, while keeping the study analytic. This deepens the understanding of the fluctuation physics by only taking into account the relevant operators. Moreover, it is also of great interest for low energy effective models. Thirdly, we discuss full unquenching effects in terms of the matter back-coupling to the glue sector that is important for QCD regimes with dominant quark fluctations such as QCD at high densities or many flavours.

The paper is organised as follows: In Sect. II we introduce the ansatz for the quantum effective action which we are considering in the present work. The general framework of dynamical hadronisation is then discussed in detail in Sect. III, where we also give a discussion of the RG flow in the gauge sector and the role of the quark-gluon vertex. Our results for two-flavour QCD are then presented in Sect. IV. While our analysis suggests that the use of dynamical hadronisation techniques only yields mild quantitative corrections in low-energy model studies, its use is indispensable from both a qualitative and a quantitative point of view for a unified description of the dynamics of QCD on all scales. Our conclusions are given in Sect. V. Some technical details as well as a brief discussion about the effect of dynamical hadronisation on low-energy models are discussed in the appendices.

II. THE EFFECTIVE ACTION

Our aim is to describe two-flavour QCD in $d = 4$ Euclidean dimensions at vanishing temperature and density in a vertex expansion. The starting point is the microscopic gauge fixed QCD action. Thus, we include the quark-gluon, three- and four-gluon vertices as well as the

ghost-gluon vertex and the corresponding momentum-dependent propagators. Four-quark interactions are dynamically generated at lower scales and we therefore take the scalar-pseudoscalar channel into account in our truncation. This is by far the dominant four-quark channel, as it exhibits quark condensation, see [3]. On even lower energy scales, bound state degrees of freedom appear and eventually become dynamical. To properly take this into account, we introduce a scale-dependent effective potential V_k which includes arbitrary orders of mesonic self-interactions. Since dynamics in this sector is dominated by the lightest mesons, we restrict our analysis to pions and the sigma-meson and their corresponding momentum-dependent propagators. Explicit chiral symmetry breaking is included via a source term $-c\sigma$. It is directly related to a finite current quark mass and, as a consequence, non-zero pion masses. This implies that we have a chiral crossover transition rather than a second order phase transition. The meson sector is coupled to the quark sector by a field-dependent Yukawa coupling $h_k(\phi^2)$. That way, arbitrarily high orders of quark-antiquark multi-meson correlators are included [27]. We elaborate on the physics picture in Sect. IV. The key mechanism to consistently describe the dynamical generation of bound state degrees of freedom in this work is dynamical hadronisation, and is discussed in Sect. III A. In summary, this yields the following scale-dependent effective action,

$$\begin{aligned}\Gamma_k = &\int_x \left\{ \frac{1}{4} F^a_{\mu\nu} F^a_{\mu\nu} + \bar{c}^a \partial_\mu D^{ab}_\mu c^b + \frac{1}{2\xi} (\partial_\mu A^a_\mu)^2 \right\} + \Delta\Gamma_{\rm glue} \\ &+ \int_x \left\{ Z_{q,k}\, \bar{q}\, (\gamma_\mu D_\mu)\, q - \lambda_{q,k} \left[(\bar{q}\, T^0 q)^2 - (\bar{q}\gamma_5 \vec{T} q)^2 \right] \right. \\ &+ h_k(\phi^2) \left[\bar{q} (i\gamma_5 \vec{T}\vec{\pi} + T^0 \sigma) q \right] + \frac{1}{2} Z_{\phi,k} (\partial_\mu \phi)^2 \\ &\left. + V_k(\rho) - c\sigma \right\}, \end{aligned} \tag{1}$$

with the $O(4)$ meson field $\phi = (\sigma, \vec{\pi})$ and $\rho = \phi^2/2$. $D_\mu = \partial_\mu - i Z^{1/2}_{A,k}\, g_k A^a_\mu t^a$ is the Dirac operator, with the strong coupling $g_k = \sqrt{4\pi\alpha_{s,k}}$ and the gluonic wave-function renormalisation $Z_{A,k}$. With this definition the covariant derivative D_μ is renormalisation group invariant. The last term in the first line, $\Delta\Gamma_{\rm glue}$, stands for the fluctuation-induced part of the full momentum-dependence of ghost and gluon propagators as well as non-trivial ghost-gluon, three-gluon and four-gluon vertex corrections, for details see [25, 28, 29].

Due to asymptotic freedom the effective action at the initial cutoff scale Λ relates to the classical (gauge-fixed) QCD action,

$$\begin{aligned}\Gamma_{k\to\Lambda} \simeq \int_x \left\{ \frac{1}{4} F^a_{\mu\nu} F^a_{\mu\nu} + \bar{q} \left(\gamma_\mu D_\mu + m_q^{\rm UV} \right) q \right. \\ \left. + \bar{c}^a \partial_\mu D^{ab}_\mu c^b + \frac{1}{2\xi} (\partial_\mu A^a_\mu)^2 \right\}. \end{aligned} \tag{2}$$

The quark mass $m_q^{\rm UV}$ at the UV scale Λ is directly related to the coupling c in Eq. (1), see also our discussion below. The other couplings appearing in our ansatz (1) for the effective action are generated dynamically in the RG flow.

In this work, we use Hermitian gamma matrices so that

$$\{\gamma_\mu, \gamma_\nu\} = 2\delta_{\mu\nu} \mathbb{1}\,. \tag{3}$$

The commutator for the $SU(N_c)$ generators reads $[t^a, t^b] = i f^{abc} t^c$ and, hence, the trace is positive, $\mathrm{Tr}\, t^a t^b = \frac{1}{2}\delta^{ab}$. $\vec{T}$ are the $SU(N_f)$ generators and $T^0 = \frac{1}{\sqrt{2N_f}} \mathbb{1}_{N_f \times N_f}$. For the field strength tensor we use the relation

$$\begin{aligned} F^{ab}_{\mu\nu} &= \frac{i}{Z^{1/2}_{A,k} g_k} [D^a_\mu\,,\, D^b_\nu] \\ &= Z^{1/2}_{A,k} \left(\partial_\mu A^a_\nu - \partial_\nu A^a_\mu + Z^{1/2}_{A,k}\, g_k f^{abc} A^b_\mu A^c_\nu \right). \end{aligned} \tag{4}$$

For more details on the gauge part of our truncation see Sect. III C.

The non-trivial momentum dependence of the quark and meson propagators is encoded by the, in general, scale-, momentum- and field-dependent wave-function renormalisations Z_q and Z_ϕ. We restrict them to be only RG-scale dependent. This approximation already captures well the non-trivial momentum dependence of the propagators [30].

All masses, wave-function renormalisations and couplings are scale-dependent. The scalar potential and the Yukawa coupling are expanded about a scale-independent point κ, $\partial_t \kappa = 0$. As shown in [27] this yields a rapid convergence of the expansion

$$\begin{aligned} V_k(\rho) &= \sum_{n=1}^{N_V} \frac{v_{n,k}}{n!} (\rho - \kappa)^n\,, \\ h_k(\rho) &= \sum_{n=0}^{N_h} \frac{h_{n,k}}{n!} (\rho - \kappa)^n\,. \end{aligned} \tag{5}$$

Note that the quark and meson mass functions (two-point functions at vanishing momentum) depend on the meson fields. The physical masses are given by the mass functions evaluated at the physical minimum $\rho_{0,k} = \sigma_0^2/2$ of $V_k(\rho) - c\sigma$,

$$\begin{aligned} m^2_{q,k} &= \frac{1}{2} h^2_k(\rho_{0,k}) \rho_{0,k}\,, \\ m^2_{\pi,k} &= V'(\rho_{0,k})\,, \\ m^2_{\sigma,k} &= V'(\rho_{0,k}) + 2\rho_{0,k} V''(\rho_{0,k})\,, \end{aligned} \tag{6}$$

where $m_{q,k}$ is the constituent quark mass. The current quark mass $m_q^{\rm UV}$ is related to the symmetry breaking

source c via the mass function at the ultraviolet scale,

$$m_q^{\rm UV} = \frac{h_\Lambda}{2v_{1,\Lambda}} c\,, \tag{7}$$

while c does not occur explicitly in the flow equation as it is the coefficient of a one-point function. This entails that the flows of the effective action in the chiral limit and that in QCD with non-vanishing current quark masses agree, see also [27]. The difference solely relates to the solution of the equation of motion for the σ-field,

$$\left.\frac{\delta\Gamma_{k=0}}{\delta\sigma}\right|_{\sigma=\sigma_{\rm EoM}} = 0\,. \tag{8}$$

If expanding the flow in powers of the mesonic fields as done in the present work, the expansion point has to be close to $\sigma_{\rm EoM}$, such that it is within the radius of convergence of the expansion.

III. QUANTUM FLUCTUATIONS

Quantum fluctuations are computed with the functional renormalisation group. For QCD related reviews and corresponding low-energy models, we refer the reader to Refs. [5–14]. A consistent description of the dynamical transition from quark-gluon degrees of freedom to hadronic degrees of freedom is achieved by the dynamical hadronisation technique. Loosely speaking, it is a way of storing four-quark interaction channels, which are resonant at the chiral phase transition, in mesonic degrees of freedom and therefore allows for a unified description of the different degrees of freedom governing the dynamics at different momentum scales.

A. Functional RG & dynamical hadronisation

The starting point of the functional renormalisation group is the scale-dependent effective action Γ_Λ at a UV-cutoff scale Λ. In the case of QCD, Λ is a large, perturbative energy scale and correspondingly Γ_Λ is the microscopic QCD action with the strong coupling constant and the current quark masses as the only free parameters of the theory. From there, quantum fluctuations are successively included by integrating out momentum shells down to the RG scale k. This yields the scale-dependent effective action Γ_k, which includes all fluctuations from momentum modes with momenta larger than k. By lowering k we resolve the macroscopic properties of the system and eventually arrive at the full quantum effective action $\Gamma = \Gamma_{k=0}$. The RG evolution of the scale-dependent effective action is given by the Wetterich equation [31], which in the case of QCD with $\Phi = (A, q, \bar{q}, c, \bar{c}, \phi)$ reads

$$\begin{aligned}\partial_t\Gamma_k[\Phi] = &\\ &\frac{1}{2}{\rm Tr}\big(G_{AA,k}[\Phi]\cdot\partial_t R_k^A\big) - {\rm Tr}\big(G_{c\bar{c},k}[\Phi]\cdot\partial_t R_k^c\big)\\ &- {\rm Tr}\big(G_{q\bar{q},k}[\Phi]\cdot\partial_t R_k^q\big) + \frac{1}{2}{\rm Tr}\big(G_{\phi\phi,k}[\Phi]\cdot\partial_t R_k^\phi\big).\end{aligned} \tag{9}$$

Here, ∂_t is the total derivative with respect to the RG scale $t = \ln(k/\Lambda)$ with some reference scale Λ. The traces sum over discrete and continuous indices of the fields, including momenta and species of fields. The first line on the right hand side of (9) is the flow in the pure glue sector, the second line creates the matter fluctuations. $G_k[\Phi]$ denote the scale and field-dependent full propagators of the respective fields, e.g.

$$(G^{-1}[\Phi])_{q\bar{q},k} = \frac{\delta^2\Gamma_k[\Phi]}{\delta q(-p)\delta\bar{q}(p)} + R_k. \tag{10}$$

In the following, we will not encounter mixed two-point functions. Hence, it is sufficient to define these expression for the combinations quark–anti-quark, meson-meson, gluon-gluon (both transverse) and ghost–anti-ghost. For the rest of the manuscript, we drop the redundant second field-index for the two-point functions, wave-function renormalisations and the propagators. In a slight abuse of notation we define the scalar parts of the two-point functions of the quark, meson, gluon and ghost as

$$\begin{aligned}\Gamma^{(2)}_{q,k}(p) &\equiv \frac{\delta^2\Gamma_k[\Phi]}{\delta q(-p)\delta\bar{q}(p)}\,,\ \Gamma^{(2)}_{\phi,k}(p) \equiv \frac{\delta^2\Gamma_k[\Phi]}{\delta\phi(-p)\delta\phi(p)}\,,\\ \Gamma^{(2)}_{A,k}(p) &\equiv \frac{\delta^2\Gamma_k[\Phi]}{\delta A(-p)\delta A(p)}\,,\ \Gamma^{(2)}_{c,k}(p) \equiv \frac{\delta^2\Gamma_k[\Phi]}{\delta c(-p)\delta\bar{c}(p)}\,,\end{aligned} \tag{11}$$

and their corresponding wave-function renormalisations and (scalar parts of the) propagators

$$\begin{aligned}Z_{\Phi_i,k}(p) &\simeq \Delta\Gamma^{(2)}_{\Phi_i,k}(p)/\Delta S^{(2)}_{\Phi_i}(p)\,,\\ G_{\Phi_i,k}(p) &\simeq \Big(Z_{\Phi_i,k}(p)\Delta S^{(2)}_{\Phi_i} + R_k^{\Phi_i}(p)\Big)^{-1}\end{aligned} \tag{12}$$

with $\Phi_i = q, \phi, A$ or c. In (12) we have $\Delta\Gamma^{(2)}_{\Phi_i,k}(p) = \Gamma^{(2)}_{\Phi_i,k}(p) - \Gamma^{(2)}_{\Phi_i,k}(0)$ for all fields except for the gluon, where $\Delta\Gamma^{(2)}_{A,k}(p) = \Gamma^{(2)}_{A,k}(p)$. The same holds true for $\Delta S^{(2)}_{\Phi_i}$. At $k = 0$ and the fields set to their vacuum expectation value, $G_{\Phi_i,k=0}(p)$ is the full propagator. For our calculations, we use four-dimensional Litim regulators R_k, [32], for details see App. C.

In the infrared regime of QCD, the dynamical degrees of freedom are hadrons, while quarks and gluons are confined inside hadrons. This entails that a formulation in terms of local composite fields with hadronic quantum numbers is more efficient in this regime. Note that these composite fields are directly related to hadronic observables at their poles.

Let us illustrate this at the relevant example of the

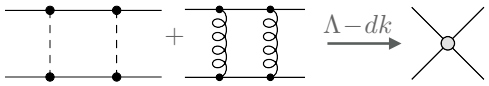

Figure 1: Re-generation of four-quark interactions from the RG-flow.

scalar-pseudoscalar mesonic multiplet at a given cutoff scale k. At a fixed large cutoff scale, where the mesonic potential $V_k(\rho)$ is assumed to be Gaußian, we can resort to the conventional Hubbard-Stratonovich bosonisation: the local part of the scalar–pseudo-scalar channel of the four-quark interaction with coupling $\lambda_{q,k}$, see the second line in (1), can be rewritten as a quark-meson term, see the third line in (1), on the equations of motion for ϕ, that is $\phi_{\rm EoM}$. This leads to

$$\lambda_{q,k} = \frac{h_k^2}{2v_{1,k}}\,, \qquad \phi_{j,\rm EoM} = \frac{h_k}{v_{1,k}}\bar{q}\boldsymbol{\tau}_j q\,, \tag{13}$$

where v_1 is the curvature mass of the mesonic field and $\boldsymbol{\tau} = (\gamma_5\vec{T}, iT^0)$, $j \in \{1,2,3,4\}$. Note that (13) is only valid for $Z_\phi \equiv 0$ and a Gaußian potential $V_k(\rho) = v_1\rho$. Moreover, mis-counting of degrees of freedom may occur from an inconsistent distribution of the original four-fermi interaction strength to the Yukawa coupling and the four-fermi coupling. The dynamical hadronisation technique used in the present work, and explained below, resolves these potential problems.

One advantage of the bosonised formulation concerns the direct access to spontaneous chiral symmetry breaking via the order parameter potential $V_k(\rho)$: spontaneous symmetry breaking is signaled by $v_1 = 0$ at the symmetry breaking scale k_χ which relates to a resonant four-quark interaction. It also facilitates the access to the symmetry-broken infrared regime.

Let us now assume that we have performed the above complete bosonisation at some momentum scale $k \gg k_\chi$. There, the above conditions for the bosonisation in (13) are valid. Hence, we can remove the four-fermi term completely in favour of the mesonic Yukawa sector. However, four-quark interactions are dynamically re-generated from the RG flow via quark-gluon and quark-meson interactions, see Fig. 1.

Indeed, these dynamically generated contributions dominate due to the increase of the strong coupling $\alpha_{s,k}$ for a large momentum regime, leading to a quasi-fixed point running of the Yukawa coupling, see Refs. [3, 22, 23] and also our discussions below. Thus, even though $\lambda_{q,k}$ was exactly replaced by $m_{\phi,k}$ and h_k at a scale $k \gg k_\chi$, there is still a non-vanishing RG-flow of $\lambda_{q,k}$ at lower scales. Note, however, that we have explicitly checked that this is only a minor quantitative effect as long as one considers low-energy effective models, see App. A.

In summary, it is not possible to capture the full dynamics of the system in the quark-gluon phase with the conventional Hubbard-Stratonovich bosonisation. As a consequence, within conventional bosonisation, the scale where composite fields take over the dynamics from fundamental quarks and gluons is not an emergent scale generated by the dynamics of QCD, but is fixed by hand by the scale where the Hubbard-Stratonovich transformation is performed.

In the present approach we employ dynamical hadronisation instead of the conventional bosonisation. It is a formal tool that allows for a unified description of dynamically changing degrees of freedom and consequently is not plagued by the shortcomings of conventional bosonisation discussed above. It has been introduced in [22] and was further developed in [7, 23, 24]. The construction works for general potentials $V_k(\rho)$ (more precisely general $\Gamma_k[\Phi]$), and implements the idea of bosonising multi-fermion interactions at every scale k rather just at the initial scale. Consequently, the resulting fields of this bosonisation procedure, i.e. the mesons, become scale-dependent and can be viewed as hybrid fields: while they act as conventional mesons at low energies, they encode pure quark dynamics at large energy scales.

Here we follow the dynamical hadronisation set-up put forward in [7] and outline the derivation of the flow equation in the presence of scale-dependent meson fields. The starting point is the functional integral representation of the scale-dependent effective action Γ_k with scale-dependent meson fields. To this end, we define the dynamical superfield $\hat{\Phi}_k = (\hat{\varphi}, \hat{\phi}_k)$, where the microscopic fields are combined in $\hat{\varphi} = (\hat{A}_\mu, \hat{q}, \hat{\bar{q}}, \hat{c}, \hat{\bar{c}})$ and the scale-dependent meson fields, in our case pions and the sigma meson, are represented by the $O(4)$ field $\hat{\phi}_k = (\hat{\vec{\pi}}_k, \hat{\sigma}_k)$. The path integral representation of Γ_k reads

$$\begin{aligned} e^{-\Gamma_k[\Phi_k]} = \int \mathcal{D}\hat{\varphi}\, \exp\Big\{ &-S[\hat{\varphi}] - \Delta S_k[\hat{\Phi}_k] \\ &+ \frac{\delta(\Gamma_k + \Delta S_k)}{\delta\Phi_k}(\hat{\Phi}_k - \Phi_k) + \Delta S_k[\Phi_k] \Big\}\,, \end{aligned} \tag{14}$$

where we defined the expectation value of the fields $\Phi_k = \langle\hat{\Phi}_k\rangle$ and used

$$J = \frac{\delta\left(\Gamma_k + \Delta S_k\right)}{\delta\Phi_k} \quad \text{and} \quad \Delta S_k[\Phi_k] = \frac{1}{2}\Phi_k R_k \Phi_k\,. \tag{15}$$

To arrive at the evolution equation for $\Gamma_k[\Phi_k]$, we take the scale derivative $\partial_t = k\frac{d}{dk}$ of Eq. (14). The RG evolution of the scale-dependent composite meson fields is of the form

$$\partial_t\hat{\phi}_k = \dot{A}_k\bar{q}\boldsymbol{\tau}q + \dot{B}_k\hat{\phi}_k\,. \tag{16}$$

For now, the coefficients $\dot{A}_k$ and $\dot{B}_k$ remain unspecified. Note that the right hand side of (16) only involves the quark mean fields $q = \langle\hat{q}\rangle$, $\bar{q} = \langle\hat{\bar{q}}\rangle$. This leads to the following identity for the flow of the hadronisation field

$$\langle\partial_t\hat{\phi}_k\rangle = \dot{A}_k\bar{q}\boldsymbol{\tau}q + \dot{B}_k\phi_k\,. \tag{17}$$

Taking (16) into account, the scale derivative of (14) gives a modified version of the flow equation (9). While the gauge and quark parts of the equation remain unchanged, the mesonic part now reads:

$$\begin{aligned}\partial_t\big|_\phi \Gamma_k[\Phi_k] =& \frac{1}{2}\mathrm{Tr}\left[G_{\phi\phi,k}[\Phi]\cdot\left(\partial_t R_k^\phi + 2R_k^\phi \dot{B}_k\right)\right] \\ &- \mathrm{Tr}\left[\frac{\delta\Gamma_k[\Phi]}{\delta\phi_i}\left(\dot{A}_k\bar{q}\boldsymbol{\tau_i}q + \dot{B}_k\phi_i\right)\right].\end{aligned} \tag{18}$$

The first line of (18) corresponds to the mesonic part of the flow equation (9) with a shift in the scale derivative of the regulator owing to the part of $\partial_t\phi_k$ which is proportional to ϕ_k itself. Note that (18) remains valid for the more general flow of the super-field [7]

$$\partial_t\hat{\Phi}_{i,k} = \dot{A}_{ij,k}\cdot F_{j,k}[\Phi_k] + \dot{B}_{ij,k}[\Phi]\hat{\Phi}_j\,, \tag{19}$$

where $F[\Phi_k]$ is any functional of the mean super-field Φ_k. The meson regulator has the form (see App. C)

$$R_k^\phi(p^2) = Z_{\phi,k}p^2 r_B(p^2/k^2)\,, \tag{20}$$

and its corresponding scale derivative can conveniently be written as

$$\partial_t R_k^\phi(p^2) = \left(\partial_t\big|_Z - \eta_{\phi,k}\right)R_k^\phi(p^2)\,, \tag{21}$$

with the anomalous dimension of the scale-dependent mesons,

$$\eta_{\phi,k} = -\frac{\partial_t Z_{\phi,k}}{Z_{\phi,k}}\,. \tag{22}$$

This choice of the regulator functions implies that the flow equations of RG-invariant quantities only contain the anomalous dimension which stems from the scale derivative of the regulator whereas the wave-function renormalisations drop out completely. With this, we can rewrite (18) into:

$$\begin{aligned}\partial_t\big|_\phi \Gamma_k[\Phi_k] =& \frac{1}{2}\mathrm{Tr}\left[G_{\phi\phi,k}[\Phi]\cdot\left(\partial_t\big|_Z - (\eta_{\phi,k} - 2\dot{B}_k)\right)R_k^\phi\right] \\ &- \mathrm{Tr}\left[\frac{\delta\Gamma_k[\Phi]}{\delta\phi_i}\left(\dot{A}_k\bar{q}\boldsymbol{\tau_i}q + \dot{B}_k\phi_i\right)\right].\end{aligned} \tag{23}$$

It is now obvious that the first line of the modified flow equation above gives the original flow equations without scale-dependent fields, but with a shifted meson anomalous dimension:

$$\eta_{\phi,k} \to \eta_{\phi,k} - 2\dot{B}_k\,. \tag{24}$$

The other coefficient, $\dot{B}_k$, in (16) is at our disposal, and we may use it to improve our truncation.

The second line of (18) induces additional contributions in particular to the flows of the four-quark and the Yukawa coupling, owing to the particular ansatz we made for $\partial_t\phi_k$. This allows us to specify the hadronisation procedure: we choose the coefficient $\dot{A}_k$ such that the flow of the four-quark interaction $\lambda_{q,k}$ vanishes within our truncation, $\partial_t\lambda_{q,k} = 0$. This way, all information about the multi-quark correlations are stored in the flow of the Yukawa coupling. Thus, h_k encodes the multi-quark correlations in the quark-gluon phase and the meson–constituent-quark correlations in the hadronic phase, including a dynamical transition between these different regimes.

B. Hadronised flow equations

In the following we specify the hadronisation procedure and give the resulting modified flow equations of the scale-dependent parameters of the truncation (1). These modifications are given by explicitly evaluating the second line of (18). Note that the explicit form of the modified flow equations depends on the details of our projection procedures, see also App. B.

In the following, we rescale all fields with their respective wave-function renormalisation, $\bar{\Phi} = \sqrt{Z_{\Phi,k}}\Phi$ and introduce the RG-invariant parameters

$$\begin{aligned}&\bar{g}_k = \frac{g_k}{Z_{q,k}Z_{A,k}^{1/2}}\,, \quad \bar{\lambda}_{q,k} = \frac{\lambda_{q,k}}{Z_{q,k}^2}, \quad \bar{c}_k = \frac{c}{Z_{\phi,k}}\,, \\ &\bar{\lambda}_{n,k} = \frac{\lambda_{n,k}}{Z_{\phi,k}^n}\,, \quad \bar{h}_{n,k} = \frac{h_{n,k}}{Z_{q,k}Z_{\phi,k}^{(2n+1)/2}}\,.\end{aligned} \tag{25}$$

The RG-invariant dimensionless masses are defined accordingly as

$$\bar{m}_{q,k} = \frac{m_{q,k}}{k\,Z_{q,k}} \quad \text{and} \quad \bar{m}_{\pi/\sigma,k} = \frac{m_{\pi/\sigma,k}}{k\,Z_{\phi,k}^{1/2}}\,. \tag{26}$$

Note that we rescale mesonic parameters with the wave-function renormalisation $Z_{\phi,k}$ of the scale-dependent mesons ϕ_k. The constant source c has a canonical running after rescaling, given only by the running of $Z_{\phi,k}$. Consequently, we also rescale the hadronisation functions and, in addition, define them to be dimensionless:

$$\dot{\bar{A}}_k = k^2 Z_{\phi,k}^{1/2} Z_{q,k}^{-1}\dot{A}_k\,, \qquad \dot{\bar{B}}_k = \dot{B}_k\,. \tag{27}$$

With this, we proceed now to the modified flow equations of these RG-invariant quantities.

For the flow of the four-quark interaction $\bar{\lambda}_{q,k}$ we find:

$$\begin{aligned}\partial_t\big|_\phi\bar{\lambda}_{q,k} =& 2\,\eta_{q,k}\bar{\lambda}_{q,k} + \partial_t\bar{\lambda}_{q,k}\big|_{\eta_{\phi,k}\to\bar{\eta}_{\phi,k}-2\dot{\bar{B}}_k} \\ &+ \left(\bar{h}_k(\bar{\rho}) + 2\bar{\rho}\bar{h}_k'(\bar{\rho})\frac{4N_fN_c-1}{2N_fN_c+1}\right)\dot{\bar{A}}_k\,.\end{aligned} \tag{28}$$

Here, $\partial_t\bar{\lambda}_{q,k}$ denotes the flow without dynamical hadronisation which is specified in App. B. As already discussed above, this contribution is subject to a shift in the meson anomalous dimension, indicated by $\eta_{\phi,k} \to \eta_{\phi,k} - 2\dot{\bar{B}}_k$.

Following the discussion in the previous section, we choose $\dot{\bar{A}}_k$ such that the flow of $\bar{\lambda}_{q,k}$ vanishes. This is achieved by the following choice:

$$\dot{\bar{A}}_k = -\left(\bar{h}_k(\bar{\rho}) + 2\bar{\rho}\bar{h}_k'(\bar{\rho})\frac{4N_fN_c-1}{2N_fN_c+1}\right)^{-1} \times \partial_t\bar{\lambda}_{q,k}\big|_{\eta_{\phi,k}\to\eta_{\phi,k}-2\dot{\bar{B}}_k}. \tag{29}$$

Together with the initial condition $\bar{\lambda}_{q,\Lambda}=0$, this yields

$$\partial_t\big|_\phi\bar{\lambda}_{q,k}=0. \tag{30}$$

The flow of the Yukawa coupling assumes the following form:

$$\partial_t\big|_\phi\bar{h}_k = \left(\eta_{q,k}+\frac{1}{2}\eta_{\phi,k}\right)\bar{h}_k + \partial_t\bar{h}_k\big|_{\eta_{\phi,k}\to\bar{\eta}_{\phi,k}-2\dot{\bar{B}}_k} - \frac{1}{k^2}\left(p^2+\bar{V}_k'(\bar{\rho})\right)\dot{\bar{A}}_k - \left(\bar{h}_k+2\bar{\rho}\bar{h}_k'\right)\dot{\bar{B}}_k, \tag{31}$$

where $\bar{h}_k=\bar{h}_k(\bar{\rho})$ is implied and $\partial_t\bar{h}_k$ is specified in App. B. From Eq. (29), it is now clear that the flow of the quark interaction and, therefore, all information about the multi-quark correlations within our truncation is incorporated into the flow of the hadronised Yukawa coupling.

It is left to specify the hadronisation function $\dot{\bar{B}}_k$, which also enters (31). It can be used to improve the current approximation by absorbing a part of the momentum-dependence of the mesonic wave-function renormalisation and the Yukawa coupling. This will be discussed elsewhere. Here, we use

$$\dot{B}_k\equiv 0. \tag{32}$$

We see that our hadronisation procedure enforces a vanishing four-quark interaction. The effect of four-quark correlations is then stored in the Yukawa coupling, which now serves a dual purpose: while it captures the current-quark self-interactions in the quark-gluon phase, it describes the meson–constituent-quark in the hadronic phase.

C. Gauge sector

In this section, we discuss the gauge sector of the truncation given in (1). Most importantly, this permits to distinguish the quark-gluon coupling from pure gluodynamics. This directly signals the transition from the perturbative quark-gluon regime at large momenta, where all couplings scale canonically, to the hadronic regime where non-perturbative effects are dominant.

The couplings induced from three-point functions play a dominant role in the description of interactions. Hence, we solve the flow equations for all three-point functions in QCD, the quark-gluon, three-gluon and ghost-gluon vertices. In addition, the effects from the four-gluon vertex are important [25, 26, 33]. Thus, we employ an ansatz which has proven to be accurate in previous studies [25, 26]. For the computation presented here, we take the gluon and ghost propagators from pure gauge theory as input [26, 33] and augment them by unquenching effects. In the perturbative domain this procedure is accurate, as the error is order $\alpha_{s,k}^2$. At scales below the confinement transition the gluon is gapped and therefore decouples from the dynamics.

Perturbation theory gives a direct relation between the number of gluon legs m attached to the vertex $\Gamma^{(n)}$ and the order in the strong coupling, $\Gamma^{(n)}\sim(4\pi\alpha_{s,k})^{m/2}$. Nevertheless, the RG running is different, although purely induced by the external legs attached. Their wave-function renormalisations cancel exactly those from the propagators, see (35) below. As a result of this truncation, the flow equations for couplings depend on the anomalous dimensions only, see below.

In this analysis we restrict ourselves to classical tensor structures of the gauge action $S[\Phi]$. Omitting colour and Lorentz indices for clarity, we parametrise the quark-gluon, three- and four-gluon and the ghost-gluon vertices as

$$\begin{aligned}\Gamma_k^{(\bar{q}Aq)} &= Z_{A,k}^{\frac{1}{2}}Z_{q,k}\,g_{\bar{q}Aq,k}\;S^{(3)}_{\bar{q}Aq},\\ \Gamma_k^{(A^3)} &= Z_{A,k}^{\frac{3}{2}}\,g_{A^3,k}\;S^{(3)}_{A^3},\\ \Gamma_k^{(A^4)} &= Z_{A,k}^{2}\,g^2_{A^4,k}\;S^{(4)}_{A^4},\\ \Gamma_k^{(\bar{c}Ac)} &= Z_{A,k}^{\frac{1}{2}}Z_{c,k}\,g_{\bar{c}Ac,k}\;S^{(3)}_{\bar{c}Ac}.\end{aligned} \tag{33}$$

The classical tensor structures $S^{(n)}_{\Phi_1\dots\Phi_n}$ are obtained from (2) by

$$S^{(n)}_{\Phi_1\dots\Phi_n} = \frac{\delta^n\Gamma_\Lambda}{\delta\Phi_1\dots\delta\Phi_n}\bigg|_{g_k=1}, \tag{34}$$

where we have omitted indices for clarity.

In this work, we use as input the gluon/ghost two-point functions $\Gamma^{(2),\mathrm{YM}}_{A/c,k}(p)$ computed in [26, 33]. In order to make full use of this non-trivial input, we expand the flow equation for the gluon propagator in QCD about that in Yang-Mills theory. We use the freedom in defining the cutoff function R_k^A, see App. C, to simplify the analysis. This is done by choosing the same prefactor $Z_{A,k}$ for the gluon regulator as for the vertex parametrisations in (33). Note that the gluon propagator enters in loop integrals with momenta $p^2\lesssim k^2$. If we estimate the full gluon propagator (12) with the simple expression

$$G_{A,k}(p)\approx\frac{1}{Z_{A,k}\,p^2+R_k^A}=\frac{1}{Z_{A,k}}\,\frac{1}{p^2\,(1+r_B(p^2/k^2))}, \tag{35}$$

i.e. the p-dependence of $Z_{A,k}(p)$ is neglected but evaluated at $p=k$, the system of flow equations considered is tremendously simplified. The error of such a simple

estimate relates to

$$p^3\left(\frac{1}{Z_{A,k}(p^2)p^2+R_k^A}-\frac{1}{Z_{A,k}p^2+R_k^A}\right)^n$$
$$=p^{3+2n}\left(\frac{Z_{A,k}-Z_{A,k}(p^2)}{\left(Z_{A,k}(p^2)p^2+R_k^A\right)\left(Z_{A,k}p^2+R_k^A\right)}\right)^n, \tag{36}$$

where the factor p^3 stems from the momentum integration $\sim dp\,p^3$. The expression in (36) occurs with powers $n\geq 1$ in the difference of the full flow equations and the approximated flows with (35), and is evaluated for momenta $p^2\lesssim k^2$. For small momenta it tends towards zero while its value for maximal momenta $p^2\approx k^2$ is proportional to the difference $Z_{A,k}-Z_{A,k}(k^2)$. Consequently, we choose

$$Z_{A,k}=Z_{A,k}(k^2)\,. \tag{37}$$

We have checked that the difference between full flows and approximated flows is less than 5% for all k.
Within approximations (33) and (35), the gluon propagator enters flow equations only via the anomalous dimension $\eta_{A,k}$ with

$$\eta_{A,k}=-\frac{\partial_t Z_{A,k}}{Z_{A,k}}\,. \tag{38}$$

Most importantly, $Z_{A,k}$ does not appear explicitly, and hence flows do only depend on $\eta_{A,k}$, the vertex couplings g, masses and further couplings. Note that this is only partially due to the approximation in (35). It mainly relates to the parameterisations (33) of the vertices which stores most of the non-trivial information in the associated vertex couplings

$$\alpha_i=\frac{g_i^2}{4\pi}\,,\quad \text{with}\quad i=\bar{c}Ac\,,A^3\,,A^4\,,\bar{q}Aq\,. \tag{39}$$

This freedom directly relates to the reparametrisation invariance of the theory and hence to RG invariance. The above discussion in particular applies to the anomalous dimension itself: first, we note that the glue part $\eta_{\text{glue},k}$ of the anomalous dimension $\eta_{A,k}$ only depends on the vertex couplings:

$$\eta_{\text{glue},k}=\eta_{\text{glue},k}(\alpha_{\bar{c}Ac}\,,\alpha_{A^3}\,,\alpha_{A^4})\,. \tag{40}$$

In the semi-perturbative regime these couplings agree due to the (RG-)modified Slavnov–Taylor identities [7, 34–36], which themselves do not restrict the couplings in the non-perturbative transition regime, see Ref. [3]. In turn, in the non-perturbative regime the couplings differ already due to their different scalings with the gluonic dressing $Z_{A,k}$. For small cutoff scales $k\to 0$, this dressing diverges proportional to the QCD mass gap,

$$\lim_{k\to 0}Z_{A,k}\propto\bar{m}^2_{\text{gap}}=\frac{m^2_{\text{gap}}}{k^2}\,. \tag{41}$$

This is a slight abuse of notation since $\bar{m}^2_{\text{gap}}$ in (41) is not renormalised as the other dimensionless mass ratios $\bar{m}^2$. Here it simply relates to the wave-function renormalisation $Z_{A,k}$ defined in (37). Hence, it is not RG-invariant and should not be confused with the physical mass gap of QCD. It is related with the latter upon an appropriate renormalisation.

As a consequence, while we expect $\alpha_{\bar{c}Ac}\approx\alpha_{\bar{q}Aq}$ down to small scales, the purely gluonic couplings should be suppressed to compensate the higher powers of diverging $Z_{A,k}$ present in the vertex dressing in (33). This also entails that we may parameterise the right hand side with powers of $1/\alpha_i$. For $i=\bar{c}Ac$, $\bar{q}Aq$, for example, we expect $1/\alpha_i$. In accordance with this observation, we parameterise the difference of the various vertex couplings in η_{glue} with the gap parameter $\bar{m}_{\text{gap}}$ defined in (41) and conclude

$$\eta_{A,k}=\eta_{\text{glue},k}(\alpha_s,\bar{m}_{\text{gap}})+\Delta\eta_{A,k}(\alpha_{\bar{q}Aq},\bar{m}_q)\,, \tag{42}$$

where α_s stands for either $\alpha_{\bar{c}Ac}$ or α_{A^3}. We shall check that our results do not depend on this choice which justifies the identification of the couplings in (42). Note that this does not entail that the couplings agree but that they differ only in the regime where the glue fluctuations decouple. Moreover, in the present approximation α_{A^4} is not computed separately but identified with α_{A^3}.

A simple reduction of (42) is given by

$$\eta_{A,k}=\eta^{\text{YM}}_{A,k}+\Delta\eta_{A,k}(\alpha_{\bar{q}Aq},\bar{m}_q)\,. \tag{43}$$

This amounts to a gluon propagator, where the vacuum polarisation is simply added to the Yang-Mills propagator. This approximation has been used in an earlier work, [1, 2, 10], and subsequently in related Dyson-Schwinger works, see e.g. [37–40].

The term $\Delta\eta_{A,k}$ is the quark contribution to the gluon anomalous dimension, and is computed with

$$\Delta\eta_{A,k}=\frac{Z_{A,k}^{-1}}{3(N_c^2-1)}\left(\frac{\partial^2}{\partial p^2}\,\Pi^{\perp}(p)\cdot\right.$$
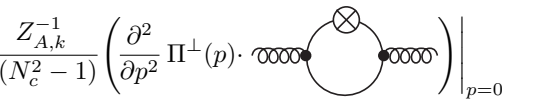
$$\left.\right)\Big|_{p=0} \tag{44}$$

Here, p is the modulus of the external momentum and $\Pi^{\perp}$ is the transversal projection operator defined in (C2). Note that the dots represent full vertices and the lines stand for full propagators. The crossed circle represents the regulator insertion. For $N_f=2$ and $N_c=3$ we find

$$\Delta\eta_{A,k}=\frac{1}{24\pi^2}\,g^2_{\bar{q}Aq,k}(1+\bar{m}^2_{q,k})^{-4}$$
$$\times\left[5-\eta_{q,k}+8\bar{m}^2_{q,k}-(1-\eta_{q,k})\bar{m}^4_{q,k}\right]. \tag{45}$$

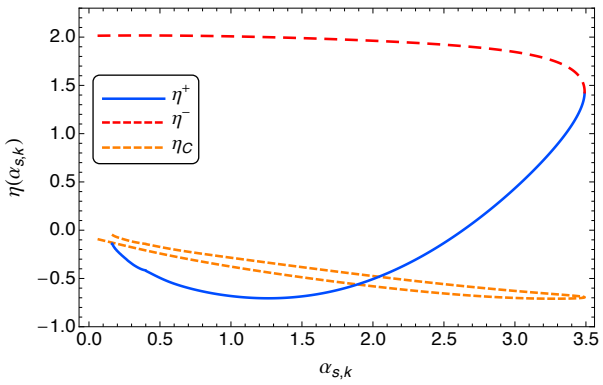

Figure 2: The UV and IR branches of $\eta_A^{\rm YM}$, η^+ and η^-, as a function of the strong coupling.

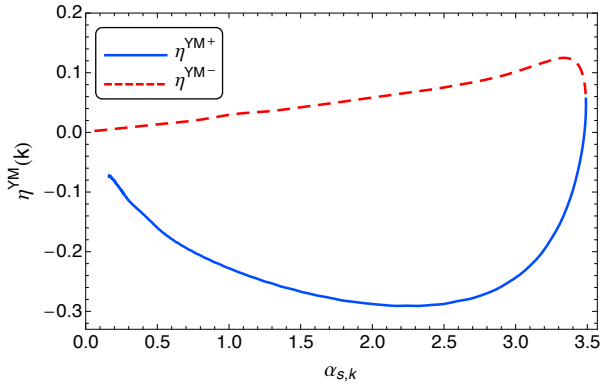

Figure 3: The UV and IR branches of $\eta_{A,k}^{\rm YM}(k)$, which is defined in (51).

The approximation (44) works well as long as the quark contribution has only a mild momentum dependence. This is the case due to the gapping of the quarks via spontaneous chiral symmetry breaking, and has been checked explicitly.

This leaves us with the task of determining $\eta_{{\rm glue},k}(\alpha_s, m_{\rm gap}^2)$, the pure glue contribution to $\eta_{A,k}$. The loop expression for $\eta_{\rm glue}$ only consists of Yang-Mills diagrams. As it depends solely on the value of the coupling α_s we arrive at

$$\eta_{\rm glue}(\alpha_s, \bar{m}_{\rm gap}^{\rm QCD}) = \eta_A^{\rm YM}(\alpha_s, \bar{m}_{\rm gap}^{\rm QCD})\,, \tag{46}$$

where $\eta_A^{\rm YM}$ can be determined in Yang-Mills theory or in quenched QCD as a function of α_s and $\bar{m}_{\rm gap}$. For using (46), of course, a trackable form of $\eta_A^{\rm YM}$ as well as $\bar{m}_{\rm gap}^{\rm QCD}$ is required.

To that end we first note that $\alpha_{s,k}$ is a multi-valued function in both Yang-Mills theory/quenched QCD and QCD, see Fig. 2. The two branches meet at $k = k_{\rm peak}$ (peak of the coupling) with

$$\partial_t \alpha_{s,k}|_{k=k_{\rm peak}} = 0\,. \tag{47}$$

We have a UV branch $\eta^+(\alpha_s, \bar{m}_{\rm gap})$ for $k > k_{\rm peak}$ and an IR branch $\eta^-(\alpha_s, \bar{m}_{\rm gap})$ for $k < k_{\rm peak}$. In Fig. 2 we show $\eta_A^{\rm YM}$ as a function of the coupling. Interestingly, $\eta^+(\alpha_{s,k})$ is well-described by a quadratic fit in α_s up to couplings close to $\alpha_{s,k_{\rm peak}}$. In turn, $\eta^-(\alpha_{s,k})$ is well-described as a function of the cutoff scale as indicated by (41) with

$$\eta^- = 2 - c^- k^2\,, \quad \text{with} \quad c^- = \frac{2 - \eta_A^{\rm YM}(\alpha_{\rm peak})}{k_{\rm peak}^2}\,, \tag{48}$$

where the mass gap $\bar{m}_{\rm gap}^2$ relates to $\eta_A^{\rm YM}(\alpha_{\rm peak})$. Note that the quality of these simple fits entails that the transition from the semi-perturbative regime to the non-perturbative IR regime happens very rapidly and asymptotic fits in both areas work very well. In summary we arrive at the final representation of $\eta_A^{\rm YM}$ with

$$\begin{aligned}\eta_{A,k}^{\rm YM} =& \eta^+(\alpha_{s,k})\theta(\alpha_{s,k} - \alpha_{s,\rm peak}) \\ &+ \eta^-(k)\theta(\alpha_{s,\rm peak} - \alpha_{s,k})\,.\end{aligned} \tag{49}$$

Inserting (49) on the right hand side of (46) gives us a closed equation for $\eta_{A,k}$ in (42). Its integration also provides us with the QCD mass gap.

The same analysis as for η_A can be applied to the ghost anomalous dimension η_c leading to a similar representation with the only difference that $\eta_{c,k=0} = 0$. It turns out that an even simpler global linear fit gives quantitatively reliable results for matter correlations,

$$\eta_{c,k}(\alpha_{s,k}) = \frac{\alpha_{s,k}}{\alpha}\eta_{c,k}^{\rm YM}(\alpha)\,, \tag{50}$$

where $\alpha_{s,k} = \alpha_{\bar{c}Ac,k}$, see Fig. 2. This modification is used in the equation for the ghost-gluon vertex. Note that this overestimates ghost-gluon correlations in the deep infrared where the glue-sector has decoupled from the matter sector. Hence this is of no relevance for the physics of chiral symmetry breaking discussed in the present work.

We are now in a position to finally determine the ghost and gluon propagators at vanishing cutoff scale in dynamical QCD. Again, we could use the $\alpha, \bar{m}_{\rm gap}$ representation for extracting the full dressing function $Z_{A,k}(p)$ on the basis of the results. To that end, the momentum-dependent flows as functions of $\alpha, \bar{m}_{\rm gap}$ are required,

$$\eta_{A,k}^{\rm YM}(p) = -\frac{\partial_t Z_{A,k}^{\rm YM}(p)}{Z_{A,k}^{\rm YM}(p)}\,, \qquad \partial_t \Delta\Gamma_{A,k}^{(2)}(p)\,, \tag{51}$$

where $\Delta\Gamma_{A,k}^{(2)}(p)$ stands for the momentum-dependent flow of the vacuum polarisation. The first term in (51) again is well approximated in terms of a low order polynomial in α_s. This is expected because is relates directly to the standard anomalous dimension of the gluon. In Fig. 3 it

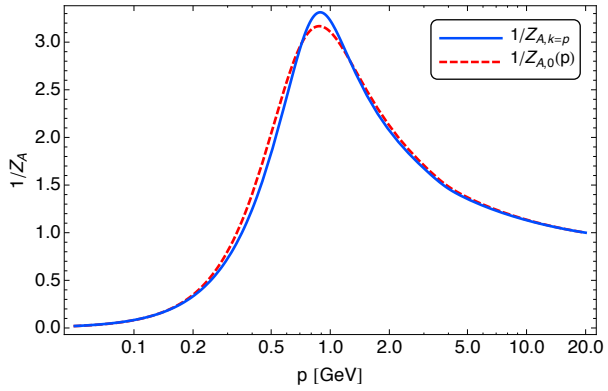

Figure 4: Comparison of the momentum dependent gluon dressing function $Z_{A,0}(p)$ and $Z_{A,k=p}$.

is shown for momentum $p = k$ as a function of $\alpha_{s,k}$.

An already very good estimate for the dressing function is

$$Z_{A,k=0}(p) \simeq Z_{A,k=p}(p) = Z_{A,k=p}\,, \tag{52}$$

as the flow of the propagators decay rapidly for momenta larger than the cutoff scale, $p \gtrsim k$. Moreover, the momentum derivative of the dressing is only large in the UV-IR transition regime. In Fig. 4, the inverse dressing $1/Z_{A,0}(p)$ and its approximation $1/Z_{A,p}$ are shown. Clearly, there are only minor deviations in the UV-IR transition regime. The same argument holds true to an even better degree for the quark contribution, and we have checked the smoothness of the flow $\Delta\Gamma_{A,k}(p)$. This leads to a very simple, but quantitative estimate for the full dressing function with

$$Z^{\rm glue}_{A/c,k=0}(p) \simeq \frac{Z^{\rm YM}_{A/c,k=0}(k_\alpha)}{Z^{\rm YM}_{A/c,k_\alpha}}\, Z^{\rm glue}_{A/c,k=p}\,, \tag{53}$$

with

$$Z^{\rm glue}_{A/c,k} = \exp\left\{-\int_\Lambda^p \frac{dk}{k}\eta^{\rm glue}_{A/c,k}\right\}\,, \tag{54}$$

where $Z_{A/c,\Lambda} = 1$, and $k_\alpha = k(\alpha_{s,k})$ is the YM-cutoff value that belongs to a given coupling α_s.

In summary we conclude that, based on Fig. 4, an already quantitative approximation to the fully unquenched propagator is done if putting the ratio in (53) to unity. This leads to

$$Z_{A/c}(p) \simeq \exp\left\{-\int_\Lambda^p \frac{dk}{k}\eta_{A/c,k}\right\}\,, \tag{55}$$

with $\eta_{A/c,k}$ defined in (42). In the non-perturbative regime diagrams involving an internal gluon are suppressed with the generated gluon mass. Hence, albeit the approximation by itself may get less quantitative in the infrared, the error propagation in the computation is small.

In summary this leaves us with relatively simple analytic flow equations for the fully back-coupled unquenching effects of glue and ghost propagators. A full error analysis of the analytic approximations here will be published elsewhere, and is very important of the reliable application of the present procedure to finite temperature and density.

In the following, we will outline the definition and derivation of the gluonic vertices we use. First of all, we only take into account the classical tensor structure of the vertices. Moreover, throughout this work, we define the running coupling at vanishing external momentum. Together with our choice for the regulators, this has the advantage that the flow equations are analytical equations. In particular, loop-momentum integrations can be performed analytically. This approximation is semi-qunatitative as long as the dressing of the classical tensor structures do not show a significant momentum dependence, and the other tensor structures are suppressed.

This approximation is motivated by results on purely gluonic vertices, see Refs. [25, 29, 41–47], which show non-trivial momentum-dependencies only in momentum regions where the gluon sector already starts to decouple from the system.

In turn, the tensor structures and momentum dependences of the quark-gluon vertex are important, see the DSE studies [48–50] and the recent fully quantitative FRG study [3]. To take this effectively into account, we introduce an infrared-strength function for the strong couplings, which is discussed below and in App. D.

To extract the flow of the quark-gluon coupling $g_{\bar{q}Aq}$, we use the following projection procedure,

$$\begin{aligned}\partial_t g_{\bar{q}Aq} = &\frac{1}{8N_f(N_c^2-1)}\\ &\times \lim_{p\to 0}\,{\rm Tr}\left(\gamma_\mu t^a \frac{\partial_t\Gamma_k}{\delta q\delta A^a_\mu \delta\bar{q}}\right)\Big|_{\Phi=\Phi_0}\,,\end{aligned} \tag{56}$$

which leads to the equation

$$\begin{aligned}\partial_t g_{\bar{q}Aq,k} = &\\ &\frac{1}{2}\left(\eta_{A,k}+2\eta_{q,k}\right)\\ &- v(d)\, g_{\bar{q}Aq,k}\,\bar{h}_k^2\left\{\mathcal{N}^{(m)}_{2,1}(\bar{m}^2_{q,k},\bar{m}^2_{\sigma,k};\eta_{q,k},\eta_{\phi,k})\right.\\ &\left.+\,(N_f^2-1)\,\mathcal{N}^{(m)}_{2,1}(\bar{m}^2_{q,k},\bar{m}^2_{\pi,k};\eta_{q,k},\eta_{\phi,k})\right\}\\ &+ g^3_{\bar{q}Aq,k}\,\frac{12v(d)}{N_{\rm c}}\,\mathcal{N}^{(g)}_{2,1}(\bar{m}^2_{q,k};\eta_{q,k},\eta_{A,k})\\ &+ g^2_{\bar{q}Aq,k}\,g_{A^3,k}\,3v(d)N_{\rm c}\,\mathcal{N}^{(g)}_{1,2}(\bar{m}^2_{q,k};\eta_{q,k},\eta_{A,k})\,.\end{aligned} \tag{57}$$

The threshold functions appearing on the right-hand side can be found in the App. C. For the quark-gluon vertex, no ghost diagrams are present. Furthermore, the mesonic contributions dominate in the infrared. These

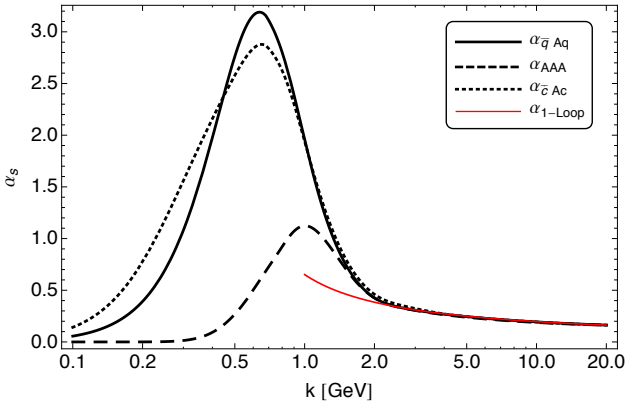

Figure 5: The running of the different strong couplings in comparison to the 1-loop running.

contributions have the same sign as the gluonic ones and therefore lead to an effective infrared enhancement of the quark-gluon vertex. The three-gluon vertex $g_{A^3,k}$ is defined via

$$\partial_t g_{A^3,k} = \frac{i}{12N_c(N_c^2-1)} \lim_{p\to 0} \frac{\partial^2}{\partial p^2} \operatorname{Tr}\left(\delta_{\mu\nu} p_\sigma f^{abc} \frac{\partial_t \Gamma_k}{\delta A(p)^a_\mu \delta A(-p)^b_\nu \delta A^c_\sigma(0)}\right)\Big|_{\Phi=\Phi_0} . \tag{58}$$

Note that in the limit of vanishing external momentum the flow is independent of the kinematic configuration in the projection procedure. Thus, we find for the flow equation for $N_c = 3$ and $N_f = 2$

$$\begin{aligned}\partial_t g_{A^3,k} = {} & \frac{3}{2}\eta_{A,k}\, g_{A^3,k} \\ & - \frac{1}{6\pi^2} g^3_{\bar{q}Aq,k} \left(1-\frac{\eta_{q,k}}{4}\right) \frac{(1+2\bar{m}^2_{q,k})}{(1+2\bar{m}^2_{q,k})^4} \\ & + \frac{3}{64\pi^2} g^3_{A^3,k} (11-2\eta_A) \\ & + \frac{1}{64\pi^2} g^3_{\bar{c}Ac,k} \left(1-\frac{\eta_{C,k}}{8}\right) ,\end{aligned} \tag{59}$$

with the ghost anomalous dimension $\eta_{C,k} = -(\partial_t Z_{C,k}(k^2))/Z_{C,k}(k^2)$. The second line in (59) corresponds to the quark-triangle diagram and the third and fourth line are the gluon- and ghost-triangle diagrams, respectively. Note that the third line also includes the contribution from the diagram containing the four-gluon vertex, which we approximate as explained below.

Within our approximation, the ghost-gluon vertex $g_{\bar{c}Ac,k}$ has only canonical running since the diagrams that contribute to the flow of $g_{\bar{c}Ac,k}$ are proportional to the external momentum. Thus, at vanishing external momentum they vanish and we are left with:

$$\partial_t g_{\bar{c}Ac,k} = \left(\frac{1}{2}\eta_{A,k} + \eta_{C,k}\right) g_{\bar{c}Ac,k} . \tag{60}$$

Lastly, we comment on our approximation for the four-gluon vertex $g_{A^4,k}$. For the sake of simplicity, we restrict here to a semi-perturbative ansatz for this vertex, which ensures that $g_{A^4,k}$ has the correct perturbative running. To this end, we set

$$g^2_{A^4,k} = g^2_{A^3,k} . \tag{61}$$

This approximation is valid for $k \gtrsim 1.5$ GeV. For smaller scales, non-perturbative effects potentially lead to a different running.

The result for the different running couplings discussed here is shown in Fig. 5. While they all agree with each other and follow the perturbative running at scales $k \gtrsim 3$ GeV, non-perturbative effects induce different runnings at lower scales. In particular, the former statement is a highly non-trivial consistency check of the approximation we make here.

As discussed above, in the present study we focus on the RG flows of the most relevant couplings from a phenomenological point of view. In particular, we concentrate on the effects of fluctuations on the relevant and marginal parameters of the classical gauge action in (1). Consequently, non-classical interactions which are potentially relevant are not taken into account here. Furthermore, we only consider vertices at vanishing external momenta, although momentum dependencies may play an important quantitative role. As an example, this becomes apparent in the flow of the ghost-gluon vertex (60): while the diagrams driving the flow of $g_{\bar{c}Ac,k}$ vanish within our approximation, they give finite contributions at non-vanishing momenta. This was studied in more detail in the case of quenched QCD [3]. Indeed, it turned out that both, momentum dependencies and the inclusion of non-classical vertices, lead to large quantitative effects. It was shown there that within an extended truncation the approach put forward in the present work leads to excellent quantitative agreement with lattice QCD studies.

We take the findings in [3] as a guideline for a phenomenological modification of the gauge couplings. Effectively this provides additional infrared strength to the gauge couplings in the non-perturbative regime with $k \lesssim 2$ GeV. This additional strength is adjusted with the current quark mass at vanishing momentum. This is reminiscent to similar procedures within Dyson-Schwinger studies, see e.g. [16, 17], the details are given in App. D.

IV. RESULTS

The starting point of the present analysis is the microscopic action of QCD. We therefore initiate the RG flow at large scales, deep in the perturbative regime. The initial

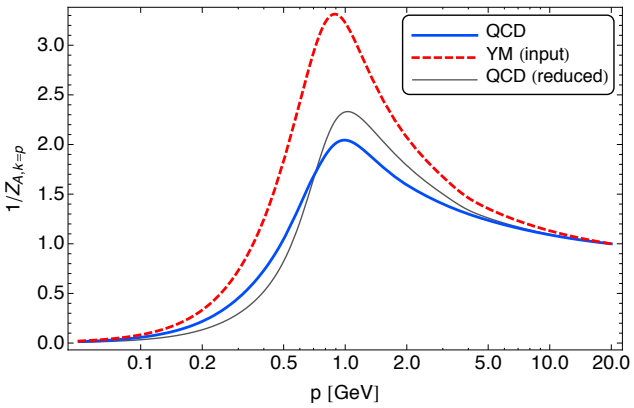

Figure 6: Comparison between the quenched and the unquenched running gluon propagators $1/Z^{\rm YM}_{A,k}(k^2)$ and $1/Z_{A,k}(k^2)$ as defined in Eq. (53). We also show the curve for QCD (reduced) where the gluon propagator is a direct sum of Yang-Mills propagator and vacuum polarisation, see Eq. (43)

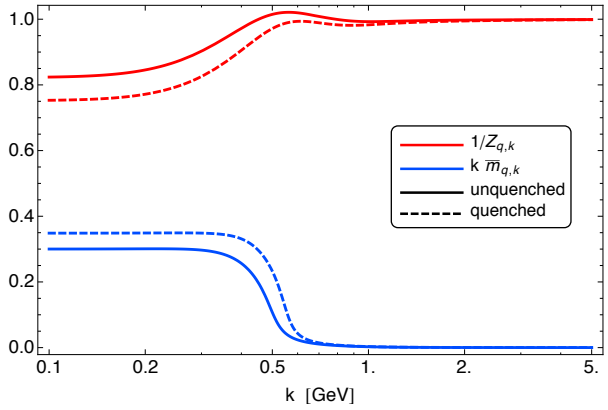

Figure 7: Dressing function (red) and mass (blue) of the quark as function of the RG scale at vanishing momentum. We compare our present model (solid) to the quenched model (dashed) with the parameters fixed to match those of [3].

values for the strong couplings are fixed by the value of the strong coupling obtained from 1-loop perturbation theory. Since the different strong couplings we use here (see Eq. (39)) need to be identical in the perturbative regime, they consequently have the same initial value α_s. It is shown in Fig. 5 that indeed the different strong couplings agree to a high degree of accuracy with the 1-loop running of the strong coupling for scales $k > 3\,\text{GeV}$. This is a very important benchmark for the consistency of the approximations we use. Note that the value of α_s implicitly determines the absolute physical scale. Here we choose $\alpha_{s,\Lambda} = 0.163$, which relates to $\Lambda \approx 20\,\text{GeV}$. A quantitative determination requires the determination of the RG-condition in relation to standard ones such as the

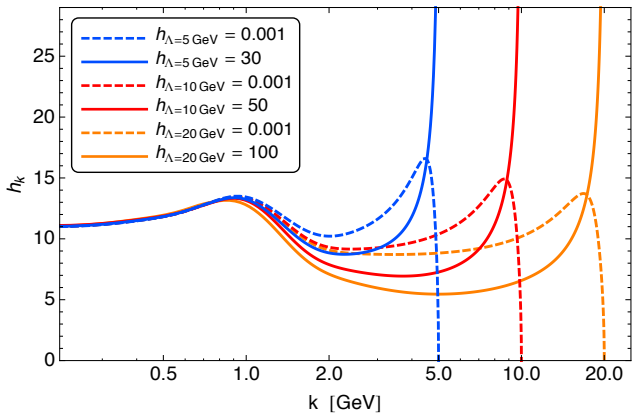

Figure 8: Yukawa coupling as a function of the RG scale for various initial scales Λ and initial conditions h_Λ.

$\bar{M}S - scheme$ as well as the extraction of $\alpha_{s,k=0}(p = \Lambda)$, using Λ as the renormalisation point. This goes beyond the scope of the present paper and we shall restrict ourselves to observables that are ratios of scales, our absolute scales are determined in terms of $\Lambda = 20$ GeV. The other microscopic parameter of QCD, the current quark mass, is in our case fixed by fixing the symmetry breaking parameter c. We choose $\bar{c}_\Lambda = 3.8\,\text{GeV}^3$ which yields a infrared pion mass of $M_{\pi,0} = 138\,\text{MeV}$; $M_k = k\bar{m}_k$ is the renormalized dimensionful mass.

Since mesons are not present in the perturbative regime, we only have to make sure that this sector is decoupled at the initial scale. We therefore choose $M^2_{\pi,\Lambda} = M^2_{\sigma,\Lambda} = 10^4\Lambda^2$. Our results are independent of the choice of the initial masses and the Yukawa coupling as long as the initial four-fermi coupling related to it is far smaller than α_s^2. This is demonstrated for the Yukawa coupling in Fig. 8, where we see that, with initial values that differ by many orders of magnitude, we always get the same solution in the IR. Loosely speaking, the memory of the initial conditions is lost in the RG flow towards the IR regime due to the presence to a pseudo fixed-point on intermediate scales, see also Ref. [23].

In the present work we have studied the unquenching effects due to the full back-coupling of the matter dynamics to the glue sector. In an earlier work,[2, 10], we directly identified $\eta_{\text{glue},k} = \eta^{\rm YM}_{A,k}$ at the same cutoff scale k, see Eq. (43). This simply adds the vacuum polarisation to the Yang-Mills propagator without feedback. It is well-adapted for taking into account qualitatively even relatively large matter contributions to the gluonic flow: the main effect of the matter back-coupling is the modification of scales, most importantly $\Lambda_{\rm QCD}$, which is already captured well in (one-loop) perturbation theory, if the initial scale is not chosen too large. This approximation has also been subsequently used in related Dyson-Schwinger works, see e.g. [37–40], extending the analysis also to finite

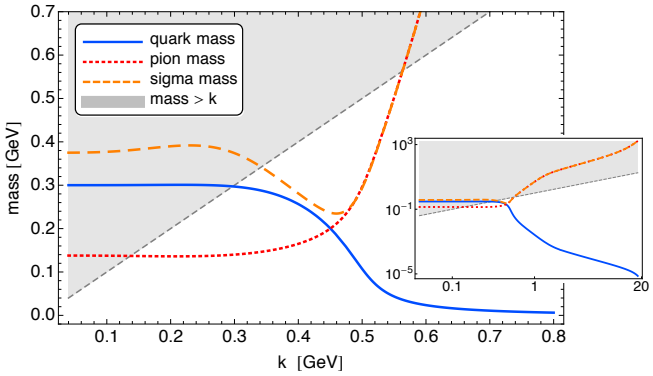

Figure 9: The renormalized quark, pion and sigma masses as a function of the RG scale. The inset figure shows the masses for a larger range of scales. The shaded gray area indicates which fields contribute dynamically: masses within the gray area exceed the cutoff scale and the corresponding fields are therefore decoupled from the dynamics. On the other hand, fields with masses within the white area are dynamical.

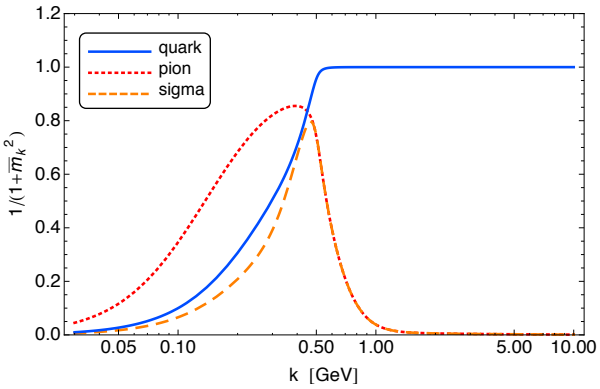

Figure 10: Dimensionless RG-invariant propagators as functions of the RG scale.

density.

In Fig. 6 we show the quenched and unquenched gluon propagators. The quenched gluon propagator is a FRG input from [26, 33]. The partially unquenched results (denoted by "QCD (reduced)" in Fig. 6) for the propagator show deviations from the fully unquenched computation. This is seemingly surprising as it is well-tested that partial unquenching works well even at finite temperature, see e.g. [2, 10, 37–40]. However, we first notice that the importance of quark flucutations is decreased at finite temperature due to the Matsubara gapping of the quarks relative to the gluons. This improves the reliability of the partial unquenching results. Moreover, in these works the infrared strength is phenomenologically adjusted with the constituent quark mass in the vacuum. This effectively accounts for the difference between unquenching and partial unquenching. Note that this finding rather supports the stability and predictive power of functional approaches.

On the other hand this also entails that the full unquenching potentially is relevant in situations where the vacuum balance between pure glue fluctuations and quark fluctuations is changed due to an enhancement of the quark fluctuations. Prominent cases are QCD with a large number of flavours, and in particular QCD at finite density. Indeed, Eq. (50) even shows the self-amplifying effect at large quark flucutations: When $\Delta\eta_q$ grows large, the ratio $\alpha_{s,\mathrm{QCD}}/\alpha_{s,\mathrm{YM}}$ decreases as does η_{glue} and the importance of the matter fluctuations is further increased. A more detailed study of this dynamics in the above mentioned situations is deferred to a subsequent publication.

For a comparison between the quenched and unquenched quark propagators see Fig. 7. We took the parameters of [3] to compute the quenched case in the present work. As in the case of the gluon propagator, Fig. 6, we see large unquenching effects. As expected, the unquenching leads to an enhancement of quark dynamics.

The present approach allows an easy access to the relative importance of quantum fluctuations of the respective fields: we find that for the renormalised, dimensionless mass being larger than one,

$$\bar{m}_\Phi^2 = \frac{m_\Phi^2}{Z_\Phi\, k^2} \geq 1\,, \tag{62}$$

all threshold functions that depend on the propagator of the respective field mode are suppressed with powers of $1/\bar{m}_\Phi^2$. This entails that the dynamics of the system is not sensitive to fluctuations of this field. In turn, for $\bar{m}_\Phi^2 \leq 1$ the field mode is dynamical. Note that, of course, $\bar{m}_\Phi^2 = 1$ is not a strict boundary for the relevance of the dynamics. In Figs. 9 and 10 we show $\bar{m}_\Phi^2$ for the matter fields. In the shaded area the condition (62) applies, and the respective matter fields do not contribute to the dynamics. This already leads to the important observation that the resonant mesonic fluctuations are only important for the dynamics in a small momentum regime with momenta $p^2 \lesssim 800$ MeV, see also Fig. 10. While the σ- and quark-modes decouple rather quickly at about 300 - 400 MeV, the $\vec{\pi}$ as a pseudo-Goldstone mode decouples at its mass scale of about 140 MeV.

In turn, in the ultraviolet regime, the mesonic modes decouple very rapidly, see Fig. 10 for the size of the propagator measured in units of the cutoff. At about 800 MeV this ratio is already 0.1 and above this scale the mesonic modes are not important, and QCD quickly is well-described by quark-gluon dynamics without resonant interactions. This observation is complementary to the fact that the initial condition of the Yukawa coupling does not play a role for the physics at vanishing coupling, see Fig. 8. For all initial cutoff scales $\Lambda \gtrsim 5$ GeV, its initial value is washed out rapidly, leading to a universal infrared regime with the prediction of $\bar{h}$ at $k = 0$.

We add that the Yukawa coupling relates to the ratio between constituent quark mass and the vacuum expec-

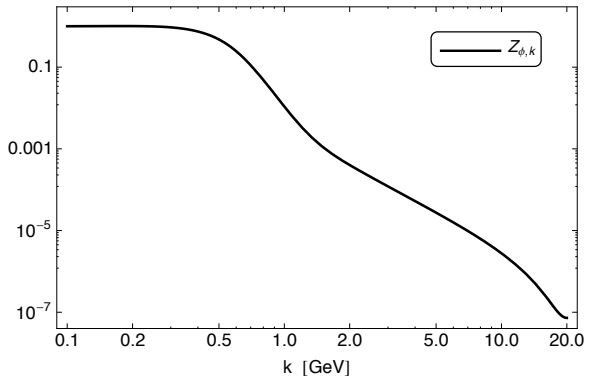

Figure 11: Wave-function renormalization of the mesons.

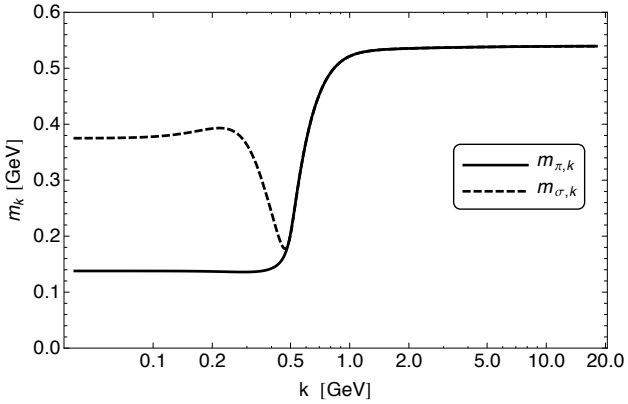

Figure 12: The masses $m_{\pi/\sigma,k} = \sqrt{\Gamma^{(2)}_{\sigma/\pi}(0)} = Z^{1/2}_{\phi,k}\bar{m}_{\pi/\sigma,k}$ of the mesons.

tation value of the field $\bar{\sigma}$,

$$\bar{h} = \frac{\bar{m}_q}{\bar{\sigma}_0}\,. \tag{63}$$

Note that it cannot be tuned and is a predicition of the theory. On the other hand, in low-energy model studies, the (renormalized) quantities $\bar{m}_q$ and $\bar{\sigma}_0$ corresponding to physical observables are related to model parameters, and have to be tuned such that $\bar{m}_q$ and $\bar{\sigma}_0$ assume their physical values.

The decoupling of meson degrees of freedom is also reflected in the behaviour of the meson wave-function renormalisation $Z_{\phi,k}$ shown in Fig. 11. Starting at scales scales $k > 500\,\mathrm{MeV}$, $Z_{\phi,k}$ decreases very rapidly towards the UV, where it is about seven orders of magnitude smaller than in the hadronic regime, where it is $\mathcal{O}(1)$. Furthermore, the masses $m^2_{\pi/\sigma,k} = \Gamma^{(2)}_{\sigma/\pi}(p^2 = 0)$ become scale-independent for $k > 800\,\mathrm{MeV}$. This implies that the meson sector becomes trivial beyond this scale. We see that the drastic decrease of the meson wave-function renormalisation triggers the large renormalised meson masses $M^2_{\pi/\sigma,k} = m^2_{\pi/\sigma,k}/Z_{\phi,k}$ shown in Fig. 9, which are responsible for the suppression of the dynamics of the meson sector at scales $k > 800\,\mathrm{MeV}$. Note that this has consequences also for low energy models in the local potential approximation, since we for scales larger than about 800 MeV, the effect of running wave-function renormalisations can not be neglected.

Finally, we discuss further consequences of our findings for low energy effective models. To that end we note that the gluon modes decouple at momenta below $500 - 700$ MeV. This is seen from the plot of the gluon dressing functions, Fig. 6, as well as that of the gluonic couplings in Fig. 5. This overlaps with the scale regime where the mesonic degrees of freedom start to dominate the dynamics.

Consequently, low energy effective models aiming at quantitative precision that do not take into account any glue fluctuations should be initiated at a UV-scale of about 500 MeV. In this regime, however, the quark-meson sector of QCD carries already some fluctuation information in non-trivial mesonic and quark-meson couplings. In other words, the standard initial effective Lagrangian of these models has to be amended by additional couplings. These couplings, however, can be computed from QCD flows.

It has been shown in [30] that in these low energy effective models thermal fluctuations affect the physics at surprisingly large scales, for thermodynamical consequences, see Ref. [51]. This is even more so for density fluctuations that lack the exponential suppression present for thermal fluctuations. Thus, we conclude that the low UV cutoff scale for quantitatively reliable low energy effective models enforces the computation of temperature- and density-dependent initial conditions. Indeed the same argument holds true for other external parameters such as the magnetic field.

V. CONCLUSIONS & OUTLOOK

In the present work, we have set up a non-perturbative FRG approach to QCD, concentrating on the effects of a full unquenching of the glue sector. We also provided a detailed study of the fluctuation physics in the transition regime from the quark-gluon phase to the hadronic phase. This includes a discussion of the relative importance of the fluctuations of quark, meson and glue fluctuations. A detailed discussion is found in the previous section.

Here we simply summarise the main results. Firstly, we have shown that the full back-coupling of the matter fluctuations in the glue sector also plays a quantitative role in the vacuum. In the present two-flavour case, it accounts for about 10-15% of fluctuation strength in the strongly correlated regime at about 1 GeV. This hints strongly at the importance of these effects in particular at finite density, where the importance of quark fluctuations is further increased and the effect is amplified.

Secondly, the still qualitative nature of the present approximation necessitates the adjustment of the infrared coupling strength, fixed with the constituent quark mass. However, the inclusion of dynamical hadronisation which re-enforces the four-fermion running, this phenomenological tuning is much reduced. In future work we plan to utilise the findings of the quantitative study [3] in quenched QCD for improving our current approximation towards quantitative precision, while still keeping its relative simplicity.

Finally, we have also discussed how low energy effective models emerge dynamically within the present set-up due to the decoupling of the glue sector: the present results and their extensions can be used to systematically improve the reliability of low energy effective models by simply computing the effective Lagrangian of these models at their physical UV cutoff scale of about 500 - 700 MeV. Moreover, the temperature- and density-dependence of the model parameters at this UV scale can be computed within the present set up.

Future work aims at a fully quantitative unquenched study by also utilising the results of [3], as well as studying the dynamics at finite temperature and density.

Acknowledgments — We are greatful to Lisa M. Haas for many discussions and collaboration in an early stage of the project. We thank Tina Herbst, Mario Mitter and Nils Strodthoff for discussions and collaboration on related projects. J.B. acknowledges support by HIC for FAIR within the LOEWE program of the State of Hesse. Moreover, this work is supported by the Helmholtz Alliance HA216/EMMI and by ERC-AdG-290623. L.F. is supported by the European Research Council under the Advanced Investigator Grant ERC-AD-267258.

Appendix A: Dynamical hadronisation and low energy effective models

In low energy models of QCD, such as (Polyakov-loop enhanced) Nambu–Jona-Lasinio models or quark-meson models, gluons are considered to be integrated out and one is left with effective four-quark interactions, either explicitly or in a bosonised formulation. The latter is particularly convenient as the phase with spontaneous broken chiral symmetry is easily accessible. There, the formulation of the effective theory is usually based on the conventional Hubbard-Stratonovich bosonization rather than dynamical hadronisation. Following our arguments given in Sect. III A, the question arises whether dynamical hadronisation leads to quantitative and/or qualitative corrections in the context of low energy effective model.

Since the matter part of our truncation (1) is that of a quark-meson model, we will consider here the special case of the quark-meson model defined by switching off all gluon contributions in (1). To see the effect of dynamical hadronisation, we look at the ratios of IR observables obtained with and without dynamical hadronisation. To this end, we choose $\Lambda_{\rm LE} = 1$ GeV as a typical UV-cutoff scale and use the same set of initial conditions in both cases. For results see Tab. I.

$f_\pi/\tilde{f}_\pi$	$M_q/\tilde{M}_q$	$M_\pi/\tilde{M}_\pi$	$M_\sigma/\tilde{M}_\sigma$
0.995	0.997	1.003	0.990

Table I: Effect of dynamical hadronisation on a quark-meson model: The quantities with/without a tilde are the results obtain from a solution of the flow equations of the quark-meson model with/without dynamical hadronisation techniques.

We see that the effect of dynamical hadronisation on physical observables of a low-energy quark-meson model (without gluons) is negligible, since it only gives corrections of less than 1%. This does not change if we vary the UV-cutoff within the range of typical values for this type of models, i.e $\Lambda_{\rm LE} \in [0.5, 1.5]$ GeV. Furthermore, it implies in particular that the mis-counting problem discussed in Sect. III A is less severe in low energy models.

This observation can be understood by looking at the flow of the four-quark interaction $\lambda_{q,k}$, see Eq. (B8). In case of the quark-meson model, only the meson box diagrams $\sim h_k^4$ contribute to the flow, see also Fig. 1, while the gluon box diagrams are neglected. In the chirally symmetric regime, the mesons are decoupled and the corresponding contributions to the flow are therefore suppressed. Furthermore, in the hadronic phase, the quarks acquire a large constituent mass and, in addition, the pions become light. Therefore, the contribution from dynamical hadronisation to the flow of the Yukawa coupling (31), $\sim \bar{m}_{\pi,k}^2 \partial_t \bar{\lambda}_{q,k}$, is suppressed by these two effects in broken phase. Thus, following our present results, in particular Fig. 9, the only regime where dynamical hadronisation can play a role in a low-energy model is in the vicinity of chiral symmetry breaking scale. However, since this region is small compared to range of scales considered even in low-energy models, only very small corrections related to the re-generation of four-quark interactions are accumulated from the RG flow.

Note, however, that we checked this statement only in vacuum and it might not be true in medium, especially at large chemical potential where quark fluctuations are enhanced. This can potentially lead to larger, non-negligible corrections from dynamical hadronisation. We also emphasise that we used the same initial conditions for our comparison of the RG flow of the quark-meson model with and without dynamical hadronisation techniques. However, usually the parameters of low-energy models are fixed in the vacuum, independent of the model truncation. Once the parameters are fixed, these models are then used to compute, e.g., the phase diagram of QCD at finite temperature and chemical potential. In this case, it may still very well be that the use of dynamical hadronisation techniques yield significant corrections.

Appendix B: Flow equations of the couplings

In this appendix, we briefly discuss the derivation of the flow equations of the couplings before dynamical hadronisation techniques are applied.

We expand the effective potential and the Yukawa coupling about a fixed expansion point κ, see (5). The advantage of such an expansion is that it is numerically stable, inexpensive and it converges rapidly [27]. This allows us to take the full field-dependent effective potential $U_k(\rho)$ and Yukawa coupling $h_k(\rho)$ into account in the present analysis.

The flow equation of the effective potential including the symmetry breaking source, $U_k(\rho) - c\sigma$, is obtained by evaluating (9) for constant meson fields, $\phi(x) \to \phi$ and vanishing gluon, quark and ghost fields. In this case, the effective action reduces to $\Gamma_k = \Omega^{-1}(U_k(\rho) - c\sigma)$, where Ω is the space-time volume. The flow of the effective potential $\bar{V}_k(\bar{\rho}) = V_k(\rho)$ is then given by:

$$\begin{aligned}&\partial_t|_\rho \bar{U}(\bar{\rho}) = \\ &2k^4 v(d)\Big\{\left[(N_f^2-1) l_0^B(\bar{m}^2_{\pi,k};\eta_{\phi,k})\right. \\ &\left. + \, l_0^B(\bar{m}^2_{\sigma,k};\eta_{\phi,k})\right] - 4N_f N_c l_1^F(\bar{m}^2_{q,k};\eta_{q,k})\Big\}\,,\end{aligned} \tag{B1}$$

where $v(d) = (2^{d+1}\pi^{d/2}\Gamma(d/2))^{-1}$. The flows of the couplings in (5) can be derived from the above equation via:

$$\begin{aligned}&\partial_{\bar{\rho}}^n\, \partial_t|_\rho \bar{U}(\bar{\rho})\Big|_{\bar{\rho}=\bar{\kappa}_k} = \\ &\quad(\partial_t - n\eta_{\phi,k})\bar{\lambda}_{n,k} - \bar{\lambda}_{n+1,k}(\partial_t + \eta_{\phi,k})\bar{\kappa}_k\,.\end{aligned} \tag{B2}$$

Rescaling the expansion point and the symmetry breaking source in order to formulate RG invariant flows introduces a canonical running for these parameters:

$$\begin{aligned}\partial_t \bar{\kappa}_k &= -\eta_\phi \bar{\kappa}_k\,,\\ \partial_t \bar{c} &= \frac{1}{2}\eta_\phi \bar{c}\,.\end{aligned} \tag{B3}$$

The renormalised minimum of the effective potential $\bar{\rho}_{0,k} = \bar{\sigma}^2_{0,k}/2$, which determines the pion decay constant at vanishing IR-cutoff, $\bar{\sigma}_{0,k=0} = f_\pi$, and serves as an order parameter for the chiral phase transition, is obtained from:

$$\partial_{\bar{\rho}}\left[\bar{U}_k(\bar{\rho}) - \bar{c}_k\bar{\sigma}\right]\Big|_{\bar{\rho}_{0,k}} = 0\,. \tag{B4}$$

All physical observables such as f_π and the masses are defined at vanishing cutoff-scale $k = 0$ and at the minimum of the effective potential $\bar{\rho} = \bar{\rho}_{0,k=0}$.

We define the field-dependent Yukawa coupling via the relation $m_{q,k}(\rho) = \sigma h_k(\rho)$ at vanishing external momentum and constant meson fields, leading to the following projection:

$$\partial_t h_k(\rho) = -\frac{1}{\sigma}\frac{i}{4N_c N_f}\lim_{p\to 0}\mathrm{Tr}\left(\frac{\delta^2\partial_t\Gamma_k}{\delta q(-p)\delta\bar{q}(p)}\right)\Big|_{\rho(x)=\rho}\,. \tag{B5}$$

The resulting flow is given by:

$$\begin{aligned}&\partial_t|_{\bar{\rho}}\bar{h}(\bar{\rho}) = \\ &\left(\eta_{q,k} + \frac{1}{2}\eta_{\phi,k}\right)\bar{h}_k(\bar{\rho}) \\ &- v(d)\bar{h}_k(\bar{\rho})^3\Big[(N_f^2-1)\, L_{1,1}^{(FB)}(\bar{M}^2_{q,k},\bar{m}^2_{\pi,k};\eta_{q,k},\eta_{\phi,k}) \\ &- \, L_{1,1}^{(FB)}(\bar{m}^2_{q,k},\bar{m}^2_{\sigma,k};\eta_{q,k},\eta_{\phi,k})\Big] \\ &+ 8v(d)\bar{h}_k(\bar{\rho})\,\bar{h}_k'(\bar{\rho})\,\bar{\rho}\left[\bar{h}_k(\bar{\rho}) + 2\bar{\rho}\bar{h}_k'(\bar{\rho})\right] \\ &\times L_{1,1}^{(FB)}(\bar{m}^2_{q,k},\bar{m}^2_{\sigma,k};\eta_{q,k},\eta_{\phi,k}) \\ &- 2v(d)k^2\left[\left(3\bar{h}_k'(\bar{\rho}) + 2\bar{\rho}\bar{h}_k''(\bar{\rho})\right) l_1^B(\bar{m}^2_{\sigma,k};\eta_{\phi,k})\right. \\ &\left. + \, 3\bar{h}_k'(\bar{\rho}) l_1^B(\bar{m}^2_{\pi,k};\eta_{\phi,k})\right] \\ &- 8(3+\xi)\, C_2(N_c)\, v(d)\, g^2_{\bar{q}Aq,k}\,\bar{h}_k(\bar{\rho}) \\ &\times L_{1,1}^{(FB)}(\bar{m}^2_{q,k},0;\eta_{q,k},\eta_{A,k})\,,\end{aligned} \tag{B6}$$

ξ is the gauge fixing parameter, which we set to zero since we use Landau gauge in this work. The flows of the renormalised couplings in (5) are:

$$\begin{aligned}&\partial_{\bar{\rho}}^n\, \partial_t|_\rho \bar{h}(\bar{\rho})\Big|_{\bar{\rho}=\bar{\kappa}_k} = \\ &\quad(\partial_t - n\eta_{\phi,k})\bar{h}_{n,k} - \bar{h}_{n+1,k}(\partial_t + \eta_{\phi,k})\bar{\kappa}_k\,.\end{aligned} \tag{B7}$$

It was shown in Ref. [27], already a ϕ^4 expansion of the effective potential, corresponding to $N_V = 2$ in (5) gives quantitatively precise results for small temperatures and densities. On the other hand, a leading order expansion of the Yukawa coupling, i.e. $N_h = 0$, is not sufficient since the expansion is not yet converged. Here, we choose $N_h = 3$ to ensure that we take the effect of the full field-dependent Yukawa coupling into account. Note that we have to choose $N_V \geq N_h$ for numerical stability and therefore choose $N_V = 5$.

For the flow of the four-quark coupling we choose the projections in [12]. This yields

$$\begin{aligned}&\partial_t\bar{\lambda}_{q,k} = \\ &- g^4_{\bar{q}Aq,k}\left(\frac{2N_c^2-3}{N_c}\right)v(d) L_{1,2}^{(FB)}(\bar{m}^2_{q,k};\eta_{q,k},\eta_{A,k}) \\ &+ \bar{h}_k(\bar{\kappa}_k)^4\left(\frac{2}{N_c}+1\right)v(d) \\ &\times L_{1,1,1}^{(FB)}(\bar{m}^2_{q,k},\bar{m}^2_{\pi,k},\bar{m}^2_{\sigma,k};\eta_{q,k},\eta_{\phi,k})\,.\end{aligned} \tag{B8}$$

In Eq. (B8), we anticipate full dynamical hadronisation for the four fermi interaction. This leads to a vanishing four-quark coupling $\bar{\lambda}_{q,k} = 0$ on the right-hand side: the self-coupling diagram proportional to $\bar{\lambda}^2_{q,k}$ is dropped.

Furthermore, we neglect contributions from higher order quark-meson vertices related to field-derivatives of $\bar{h}_k(\bar{\rho})$, since they are subleading.

The anomalous dimensions are related to the flow of the wave-function renormalisations, $\eta = -\partial_t Z/Z$. The Z's on the other hand encode the non-trivial momentum dependence of the propagators. Here, as already discussed above, we approximate the full momentum, scale and field dependence of the anomalous dimensions by only scale-dependent ones in the leading order expansion in the fields in analogy to (5):

$$Z_{\phi,k}(p^2,\rho) = Z_{\phi,k}(\kappa) \quad \text{and} \quad Z_{q,k}(p^2,\rho) = Z_{q,k}(\kappa)\,. \tag{B9}$$

For the meson anomalous dimension, we therefore use the following projection:

$$\eta_{\phi,k} = -\frac{1}{2Z_{\phi,k}} \lim_{p\to 0} \frac{\partial^2}{\partial |p|^2} \mathrm{Tr}\left(\frac{\delta^2 \partial_t \Gamma_k}{\delta\pi_i(-p)\delta\pi_i(p)}\right)\Big|_{\rho=\kappa}, \tag{B10}$$

where the choice of $i = 1,2,3$ does not matter, owing to the $O(3)$ symmetry of the pions. This yields

$$\begin{aligned}\eta_{\phi,k} = &\\ &8\, v(d) k^{-2} \bar{\kappa}_k\, \bar{U}_k''(\bar{\kappa}_k)^2\, \mathcal{M}_{2,2}(\bar{m}^2_{\pi,k}, \bar{m}^2_{\sigma,k})\\ &+ 2N_c\, N_f\, v(d)\, \bar{h}_k(\bar{\kappa}_k)^2 \left[\mathcal{M}_4(\bar{m}^2_{q,k};\eta_{q,k})\right.\\ &\left.+\frac{1}{2} k^{-2} \bar{\kappa}_k \bar{h}_k(\bar{\kappa}_k)^2 \mathcal{M}_2(\bar{m}^2_{q,k};\eta_{q,k})\right].\end{aligned} \tag{B11}$$

Note that it is crucial that the functional derivatives in (B10) are with respect to the pions, since sigma-derivatives would contaminate the flow with contributions proportional to $\sigma Z'_{\phi,k}(\rho)$.

For the anomalous dimension of quarks, we use the projection

$$\begin{aligned}\eta_{q,k} \;=\; &-\frac{1}{8N_f N_c Z_{q,k}}\\ &\times \lim_{p\to 0} \frac{\partial^2}{\partial |p|^2} \mathrm{Tr}\left(\gamma_\mu p_\mu \frac{\delta^2 \partial_t \Gamma_k}{\delta q(-p)\delta\bar{q}(p)}\right)\Big|_{\rho=\kappa},\end{aligned} \tag{B12}$$

which yields

$$\begin{aligned}\eta_q = &\\ &2\, v(d)\, C_2(N_c) g^2_{\bar{q}Aq} \left[(3-\xi)\mathcal{M}_{1,2}(\bar{m}^2_{q,k}, 0; \eta_{A,k})\right.\\ &\left.- 3(1-\xi)\tilde{\mathcal{M}}_{1,1}(\bar{m}^2_{q,k}, 0; \eta_{q,k}, \eta_{A,k})\right]\\ &+ \frac{1}{2}\, v(d)[\left(\bar{h}_k(\bar{\kappa}_k) + 2\bar{\kappa}_k \bar{h}'_k(\bar{\kappa}_k)\right)^2\\ &\times \mathcal{M}_{1,2}(\bar{m}^2_{q,k}, \bar{m}^2_{\sigma,k}; \eta_{\phi,k})\\ &+ (N_f^2 - 1)\bar{h}_k(\bar{\kappa}_k)^2\, \mathcal{M}_{1,2}(\bar{m}^2_{q,k}, \bar{m}^2_{\pi,k}; \eta_{\phi,k})\big]\,.\end{aligned} \tag{B13}$$

The corresponding threshold functions can be found in the next Appendix.

Appendix C: Threshold functions

Here, we collect the threshold functions which enter the flow equations and encode the regulator and momentum dependence of the flows. Note that it is here, where the substitution $\eta_{\phi,k} \to \eta_{\phi,k} - 2\dot{\bar{B}}_k$ has to be made according to (24).

Throughout this work, we use $4d$ regulator functions of the form:

$$\begin{aligned} R_k^{\phi}(p^2) &= Z_{\phi,k}\, p^2 r_B(p^2/k^2)\,,\\ R_k^{q}(p^2) &= Z_{q,k}\, \gamma_\mu p_\mu r_F(p^2/k^2)\,,\\ R_k^{A,\mu\nu}(p^2) &= Z_{A,k}\, p^2 r_B(p^2/k^2)\, \Pi^{\perp}_{\mu\nu}(p)\,,\end{aligned} \tag{C1}$$

with the transverse projector

$$\Pi^{\perp}_{\mu\nu}(p) = \delta_{\mu\nu} - \frac{p_\mu p_\nu}{p^2}\,. \tag{C2}$$

Note that in the approximation at hand the ghost regulator does not enter. The optimised regulator shape functions $r_{B/F}(x)$ are given by [32]:

$$\begin{aligned} r_B(x) &= \left(\frac{1}{x} - 1\right)\Theta(1-x)\,,\\ r_F(x) &= \left(\frac{1}{\sqrt{x}} - 1\right)\Theta(1-x)\,.\end{aligned} \tag{C3}$$

The threshold functions for the effective potential are

$$l_n^B(\bar{m}_B^2;\eta_B) = \frac{2(\delta_{n,0}+n)}{d}\left(1 - \frac{\eta_B}{d+2}\right)(1+\bar{m}_B^2)^{-(n+1)}\,,$$
$$l_n^F(\bar{m}_F^2;\eta_F) = \frac{2(\delta_{n,0}+n)}{d}\left(1 - \frac{\eta_F}{d+1}\right)(1+\bar{m}_F^2)^{-(n+1)}\,,$$

and that for the Yukawa coupling and the four-quark coupling are

$$L_{1,1}^{(FB)}(\bar{m}_F^2,\bar{m}_B^2;\eta_F,\eta_B)=\frac{2}{d}(1+\bar{m}_F^2)^{-1}(1+\bar{m}_B^2)^{-1}\left\{\left(1-\frac{\eta_F}{d+1}\right)(1+\bar{m}_F^2)^{-1}+\left(1-\frac{\eta_B}{d+2}\right)(1+\bar{m}_B^2)^{-1}\right\}, \tag{C4}$$

$$L_{1,2}^{(FB)}(\bar{m}_F^2;\eta_F,\eta_B)=\frac{2}{d}(1+\bar{m}_F^2)^{-2}\left\{2\left(1-\frac{2\eta_B}{d+2}\right)-\left(1-\frac{\eta_F}{d+1}\right)+2(1+\bar{m}_F^2)^{-1}\left(1-\frac{\eta_F}{d+1}\right)\right\},$$

$$\begin{aligned}L_{1,1,1}^{(FB)}(\bar{m}_F^2,\bar{m}_{B1}^2,\bar{m}_{B2}^2;\eta_F,\eta_B)=\frac{2}{d}(1+\bar{m}_F^2)^{-2}(1+\bar{m}_{B1}^2)^{-1}(1+\bar{m}_{B2}^2)^{-1}\Bigg\{&\left[(1+\bar{m}_{B1}^2)^{-1}+(1+\bar{m}_{B2}^2)^{-1}\right]\\ &\times\left(1-\frac{\eta_B}{d+2}\right)+\left[2(1+\bar{m}_F^2)^{-1}-1\right]\left(1-\frac{\eta_F}{d+1}\right)\Bigg\}.\end{aligned} \tag{C5}$$

For the anomalous dimensions, we have

$$\begin{aligned}\mathcal{M}_2(\bar{m}_F^2;\eta_F)&=\left(1+\bar{m}_F^2\right)^{-4},\\ \mathcal{M}_{2,2}(\bar{m}_{B1}^2,\bar{m}_{B2}^2;\eta_B)&=(1+\bar{m}_{B1}^2)^{-2}(1+\bar{m}_{B2}^2)^{-2}\\ \mathcal{M}_{1,2}(\bar{m}_F^2,\bar{m}_B^2;\eta_F,\eta_B)&=\left(1-\frac{\eta_B}{d+1}\right)(1+\bar{m}_F^2)^{-1}(1+\bar{m}_B^2)^{-2}\\ \mathcal{M}_4(\bar{m}_F^2;\eta_F)&=\left(1+\bar{m}_F^2\right)^{-4}+\frac{1-\eta_F}{d-2}\left(1+\bar{m}_F^2\right)^{-3}-\left(\frac{1}{4}+\frac{1-\eta_F}{2d-4}\right)\left(1+\bar{m}_F^2\right)^{-2}\\ \tilde{\mathcal{M}}_{1,1}(\bar{m}_F^2,\eta_F,\eta_B)&=\frac{2}{d-1}\left(1+\bar{m}_F^2\right)^{-1}\left\{\frac{1}{2}\left(\frac{2\eta_F}{d}-1\right)+\left(1-\frac{\eta_B}{d+1}\right)+\left(1-\frac{2\eta_F}{d}\right)\left(1+\bar{m}_F^2\right)^{-1}\right\}.\end{aligned} \tag{C6}$$

Finally, for the flow of $z_{\bar{q}Aq}$ we use

$$\begin{aligned}\mathcal{N}_{2,1}^{(m)}(\bar{m}_F^2,\bar{m}_B^2;\eta_F,\eta_B)&=\frac{1}{d}\left(1-\frac{\eta_F}{d+1}\right)(1+\bar{m}_B^2)^{-1}\left\{2\bar{m}_F^2(1+\bar{m}_F^2)^{-3}+(1+\bar{m}_F^2)^{-2}\right\}\\ &\quad+\frac{1}{d}\left(1-\frac{\eta_B}{d+2}\right)(1+\bar{m}_B^2)^{-2}\left\{\bar{m}_F^2(1+\bar{m}_F^2)^{-2}+(1+\bar{m}_F^2)^{-1}\right\},\\ \mathcal{N}_{2,1}^{(g)}(\bar{m}_F^2;\eta_F,\eta_A)&=\frac{1}{d}\left(1-\frac{\eta_F}{d+1}\right)\bar{m}_F^2(1+\bar{m}_F^2)^{-3}+\frac{1}{2d}\left(1-\frac{\eta_A}{d+2}\right)\bar{m}_F^2(1+\bar{m}_F^2)^{-2},\\ \mathcal{N}_{1,2}^{(g)}(\bar{m}_F^2;\eta_F,\eta_A)&=\frac{1}{d+1}\left(1-\frac{\eta_F}{d+2}\right)\left\{2\bar{m}_F^2(1+\bar{m}_F^2)^{-2}-(1+\bar{m}_F^2)^{-1}\right\}\\ &\quad+\frac{4}{d+1}\left(1-\frac{\eta_A}{d+3}\right)(1+\bar{m}_F^2)^{-1}.\end{aligned} \tag{C7}$$

Appendix D: Infrared parameter

In our study, we introduced an "infrared-strength" function $\varsigma_{a,b}(k)$ which we define as

$$\varsigma_{a,b}(k)=1+a\,\frac{(k/b)^\delta}{e^{(k/b)^\delta}-1}\,, \tag{D1}$$

with $b>0$ and $\delta>0$. Note that the specific form of $\varsigma_{a,b}(k)$ is irrelevant for our result as long as it has the properties specified below. It defines a smooth step function centered around b with interpolates smoothly between

$$\varsigma_{a,b}(k\gg b)=1\quad\text{and}\quad\varsigma_{a,b}(k\ll b)=1+a\,. \tag{D2}$$

Thus, for $b = \mathcal{O}(1\,\mathrm{GeV})$, $\varsigma_{a,b}(k)$ gives an IR-enhancement, while it leaves the perturbative regime unaffected. We then modify the gauge couplings as

$$g_{s,k} \longrightarrow \varsigma_{a,b}(k)\, g_{s,k}, \tag{D3}$$

where $g_{s,k} = g_{\bar{q}Aq,k}\,,\, g_{A^3,k}\,,\, g_{\bar{c}Ac,k}$. We choose the same parameters a and b for every gauge coupling. Accordingly, the flow equations of the gauge couplings then are

$$\partial_t g_{s,k} \longrightarrow g_{s,k}\, \partial_t \varsigma_{a,b}(k) + \varsigma_{a,b}(k)\, \partial_t g_{s,k}. \tag{D4}$$

We have found that our results do not depend strongly on the precise value of b as long as it is $\mathcal{O}(1\,\mathrm{GeV})$. To be specific, we choose $b = 1.3\,\mathrm{GeV}$ for $\delta = 3$ in the following.

The parameter a is adjusted such that we get physical constituent quark masses in the infrared. Here, $a = 0.47$ yields $M_{q,0} = 302\,\mathrm{MeV}$, where $M_{q,k} = k\bar{m}_{q,k}$ is the renormalized quark mass.

Since the results in Ref. [3] demonstrate that the largest source for systematic errors of our truncation is rooted in the approximations that enter the flows of the gauge couplings, a procedure as discussed above is well-justified.

[1] J. Braun, Eur. Phys. J. **C64**, 459 (2009), 0810.1727.
[2] J. Braun, L. M. Haas, F. Marhauser, and J. M. Pawlowski, Phys.Rev.Lett. **106**, 022002 (2011), 0908.0008.
[3] M. Mitter, J. M. Pawlowski, and N. Strodthoff (2014), 1411.7978.
[4] J. Braun, L. Fister, T. Herbst, M. Mitter, J. M. Pawlowski, F. Rennecke, and N. Strodthoff (fQCD Collaboration).
[5] D. F. Litim and J. M. Pawlowski, pp. 168–185 (1998), hep-th/9901063.
[6] J. Berges, N. Tetradis, and C. Wetterich, Phys. Rept. **363**, 223 (2002), hep-ph/0005122.
[7] J. M. Pawlowski, Annals Phys. **322**, 2831 (2007), hep-th/0512261.
[8] B.-J. Schaefer and J. Wambach, Phys.Part.Nucl. **39**, 1025 (2008), hep-ph/0611191.
[9] H. Gies, Lect.Notes Phys. **852**, 287 (2012), hep-ph/0611146.
[10] J. M. Pawlowski, AIP Conf.Proc. **1343**, 75 (2011), 1012.5075.
[11] O. J. Rosten (2010), 1003.1366.
[12] J. Braun, J.Phys. **G39**, 033001 (2012), 1108.4449.
[13] L. von Smekal, Nucl.Phys.Proc.Suppl. **228**, 179 (2012), 1205.4205.
[14] J. M. Pawlowski, Nucl.Phys. **A** (2014).
[15] R. Alkofer and L. von Smekal, Phys. Rept. **353**, 281 (2001), hep-ph/0007355.
[16] C. D. Roberts and S. M. Schmidt, Prog. Part. Nucl. Phys. **45**, S1 (2000), nucl-th/0005064.
[17] C. S. Fischer, J.Phys.G **G32**, R253 (2006), hep-ph/0605173.
[18] C. S. Fischer, A. Maas, and J. M. Pawlowski, Annals Phys. **324**, 2408 (2009), 0810.1987.
[19] D. Binosi and J. Papavassiliou, Phys.Rept. **479**, 1 (2009), 0909.2536.
[20] A. Maas, Phys.Rept. **524**, 203 (2013), 1106.3942.
[21] P. Boucaud, J. Leroy, A. L. Yaouanc, J. Micheli, O. Pene, et al., Few Body Syst. **53**, 387 (2012), 1109.1936.
[22] H. Gies and C. Wetterich, Phys.Rev. **D65**, 065001 (2002), hep-th/0107221.
[23] H. Gies and C. Wetterich, Phys.Rev. **D69**, 025001 (2004), hep-th/0209183.
[24] S. Floerchinger and C. Wetterich, Phys.Lett. **B680**, 371 (2009), 0905.0915.
[25] L. Fister and J. M. Pawlowski (2011), 1112.5440.
[26] L. Fister and J. M. Pawlowski, in preparation (2014).
[27] J. M. Pawlowski and F. Rennecke, Phys. Rev. D **90**, 076002 (2014), 1403.1179.
[28] L. Fister and J. M. Pawlowski, Phys.Rev. **D88**, 045010 (2013), 1301.4163.
[29] L. Fister, *doctoral thesis*, Heidelberg University, (2012), 2012.
[30] A. J. Helmboldt, J. M. Pawlowski, and N. Strodthoff (2014), 1409.8414.
[31] C. Wetterich, Phys.Lett. **B301**, 90 (1993).
[32] D. F. Litim, Phys.Lett. **B486**, 92 (2000), hep-th/0005245.
[33] C. S. Fischer, A. Maas, and J. M. Pawlowski, PoS **CONFINEMENT8**, 043 (2008), 0812.2745.
[34] U. Ellwanger, Phys. Lett. **B335**, 364 (1994), hep-th/9402077.
[35] M. D'Attanasio and T. R. Morris, Phys.Lett. **B378**, 213 (1996), hep-th/9602156.
[36] Y. Igarashi, K. Itoh, and H. So, Prog.Theor.Phys. **106**, 149 (2001), hep-th/0101101.
[37] C. S. Fischer, J. Luecker, and J. A. Mueller, Phys.Lett. **B702**, 438 (2011), 1104.1564.
[38] C. S. Fischer and J. Luecker, Phys.Lett. **B718**, 1036 (2013), 1206.5191.
[39] C. S. Fischer, L. Fister, J. Luecker, and J. M. Pawlowski, Phys.Lett. **B732**, 273 (2014), 1306.6022.
[40] C. S. Fischer, J. Luecker, and J. M. Pawlowski (2014), 1409.8462.
[41] M. Q. Huber and L. von Smekal, JHEP **1304**, 149 (2013), 1211.6092.
[42] M. Pelaez, M. Tissier, and N. Wschebor, Phys.Rev. **D88**, 125003 (2013), 1310.2594.
[43] G. Eichmann, R. Williams, R. Alkofer, and M. Vujinovic, Phys.Rev. **D89**, 105014 (2014), 1402.1365.
[44] A. Blum, M. Q. Huber, M. Mitter, and L. von Smekal, Phys.Rev. **D89**, 061703 (2014), 1401.0713.
[45] D. Binosi, D. Ibanez, and J. Papavassiliou (2014), 1407.3677.
[46] J. Gracey, Phys.Rev. **D90**, 025014 (2014), 1406.0649.
[47] A. K. Cyrol, M. Q. Huber, and L. von Smekal (2014), 1408.5409.
[48] M. Hopfer, A. Windisch, and R. Alkofer, PoS **ConfinementX**, 073 (2012), 1301.3672.
[49] R. Williams (2014), 1404.2545.
[50] A. Aguilar, D. Binosi, D. Ibanez, and J. Papavassiliou (2014), 1405.3506.
[51] T. K. Herbst, M. Mitter, J. M. Pawlowski, B.-J. Schaefer,

and R. Stiele, Phys.Lett. **B731**, 248 (2014), 1308.3621.